Probing the Catalytic Mechanism of Sulfite Reductase by X-ray Crystallography: Structures of the *Escherichia coli* Hemoprotein in Complex with Substrates, Inhibitors, Intermediates, and Products[†,‡]

Brian R. Crane,[§] Lewis M. Siegel,[||] and Elizabeth D. Getzoff*[,§]

Department of Molecular Biology and The Skaggs Institute for Chemical Biology, The Scripps Research Institute, La Jolla, California 92037, and Department of Biochemistry, Duke University Medical Center, Durham, North Carolina 27710

Received May 7, 1997; Revised Manuscript Received July 25, 1997[⊗]

ABSTRACT: To further understand the six-electron reductions of sulfite and nitrite catalyzed by the *Escherichia coli* sulfite reductase hemoprotein (SiRHP), we have determined crystallographic structures of the enzyme in complex with the inhibitors phosphate, carbon monoxide, and cyanide, the substrates sulfite and nitrite, the intermediate nitric oxide, the product sulfide (or, most likely, an oxidized derivative thereof), and an oxidized nitrogen species (probably nitrate). A hydrogen-bonded cage of ligand-binding arginine and lysine side chains, ordered water molecules, and siroheme carboxylates provides preferred locations for recognizing the common functional groups of these ligands and accommodates their varied sizes, shapes, and charged without requiring substantial structural changes. The coordination geometries presented here suggest that the successively deoxygenated sulfur and nitrogen species produced during catalysis need not alter their orientation in the active site to adopt new stable coordination states. Strong π-acid ligands decrease the bond length between the siroheme and the proximal cysteine thiolate shared with the iron−sulfur cluster, emphasizing the ability of the coupled cofactors to promote electron tranfer into substrate. On binding the siroheme, the substrate sulfite provides an oxygen atom in a unique location of the binding site compared to all other ligands studied, induces a spin transition in the siroheme iron, flips an active-site arginine, and orders surrounding active-center loops. The loop that coalesces over the active center shields the positively charged ligand-coordinating residues from solvent, enhancing their ability to polarize the substrate. Hydrogen bonds supplied by active-site arginine and lysine residues facilitate charge transfer into the substrate from the electron-rich cofactors, activate S−O bonds for reductive cleavage, and provide potential proton sources for the formation of favorable aquo leaving groups on the substrate. Strong interactions between sulfite and ordered water molecules also implicate solvent as a source of protons for generating product water. From the structures reported here, we propose a series of key structural states of ligated SiRHP in the catalytic reduction of sulfite to sulfide.

Sulfite reductases (SiRs)[1] and related nitrite reductases (NiRs) are the only known class of enzymes that couple a porphyrin to an iron−sulfur cluster in a catalytically active redox center. In this center, the siroheme (tetrahydroporphyrin of the isobacteriochlorin class) and the Fe_4S_4 cluster, which are bridged by a cysteine thiolate, function cooperatively with the protein moiety to reduce sulfite to sulfide and nitrite to ammonia during the biological assimilation and dissimilation of sulfur and nitrogen compounds. To further understand the catalysis of six-electron reductions by these complex metalloenzymes, we have determined crystallographic structures of the assimilatory *Escherichia coli* sulfite reductase hemoprotein (SiRHP) in complex with substrates, inhibitors, products, and reaction intermediates.

The structure of the SiRHP active center has been optimized to associate the coupled cofactors and inorganic anions in an environment conducive for multielectron transfer from cofactors to substrate (Crane *et al.*, 1995). The siroheme and Fe_4S_4 cluster, linked by a shared cysteine thiolate ligand (Cys483), are bound at the interface of three $\alpha + \beta$ domains. β-Sheets from two of SiRHP's three domains, and the siroheme itself, form the walls of a cavity close to the molecular surface where substrates, inhibitors, and associated water molecules interact with the protein. Coordination of substrate and inhibitor anions to the remaining distal axial coordination of the siroheme is aided by positively charged protein residues that extend from the surrounding β-strands. Specifically, Arg83, Arg153, Lys215, and Lys217 directly hydrogen-bond to the oxygen atoms of bound anions. These residues, along with Arg117 and Arg214, produce a high effective proton concentration above

[†] This work was supported by NIH Grants GM37684 to E.D.G. and GM212226 to L.M.S. and an NSERC 1967 fellowship to B.R.C.

[‡] PDB codes for the structures reported herein: HP−SO_3, 2GEP; HP−NO_2, 3GEO; HP−CN, 4GEP; HP−CO, 5GEP; HP−NO, 6GEP; HP−S, 7GEP; HP−NO_3, 8GEP.

* Author to whom correspondence should be addressed.

[§] The Scripps Research Institute.

[||] Duke University Medical Center.

[⊗] Abstract published in *Advance ACS Abstracts,* September 15, 1997.

[1] Abbreviations: HEPES, *N*-(2-hydroxyethyl)piperazine-*N*′-2-ethanesulfonic acid; EDTA, ethylenediaminetetraacetic acid; EPR, electron paramagnetic resonance; Fe(TPP)(NO)(1-MeIm), nitrosyl-$\alpha,\beta,\gamma,\delta$-tetraphenyl porphinato(1-methylimidizole)iron(II); HP, oxidized sulfite reductase hemoprotein (siroheme Fe^{3+}, $Fe_4S_4^{2+}$); HP −1, one-electron reduced sulfite reductase hemoprotein (siroheme Fe^{2+}, $Fe_4S_4^{2+}$); HP −2, two-electron reduced sulfite reductase hemoprotein (siroheme Fe^{2+}, $Fe_4S_4^{1+}$); KP_i, potassium phosphate buffer, pH 7.7; NiR, nitrite reductase; 1-MeIm, 1-methylimidazole; MV+, reduced methyl viologen; PAGE, polyacrylamide gel electrophoresis; PEG, poly(ethylene glycol); SFe, siroheme iron; SiR, sulfite reductase; SiRHP, sulfite reductase hemoprotein; SNiRR, sulfite or nitrite reductase repeat; SpiaNiR, spinach assimilatory nitrite reductase; SSRL, Stanford Synchrotron Radiation Laboratory.

S0006-2960(97)01066-0 CCC: $14.00

the distal face of the siroheme, opposite to the proximal bridging ligand, Cys483. The active-site cavity and distal siroheme coordination position is accessible to solvent from a direction that is roughly perpendicular to the siroheme normal.

Complexes of SiRHP with traditional heme ligands provide insights into electronic states of the cofactors and contributing features of the protein that may be relevant for understanding catalysis. The binding of small ligands to SiRHP is governed not only by direct interaction with the siroheme and protein moiety but also by the indirect influence of the cluster and protein on the electronic state of the siroheme−ligand complex. As isolated in its oxidized state (HP), the SiRHP siroheme iron is ferric (Fe^{3+}) and the cluster cubane has a net charge of +2 ($Fe_4S_4^{2+}$). Each prosthetic group can be reduced by one electron: the siroheme iron to Fe^{2+} at a reduction potential (E_0') of −340 mV (HP −1) and the cluster to $Fe_4S_4^{1+}$ at an E_0' of −405 mV (HP −2) (Siegel *et al.*, 1982; Janick & Siegel, 1982). Cyanide forms a low-spin siroheme complex with all three oxidation states of SiRHP, whereas carbon monoxide only reacts with the ferrous siroheme (Siegel *et al.*, 1982; Janick & Siegel, 1982,1983). Coordination of a π-acceptor ligand such as cyanide stabilizes (increases) the redox potential of the siroheme by 185 mV, whereas coordination of either CN^- or CO to the siroheme destabilizes the lower iron−sulfur cluster redox potential (Janick & Siegel, 1982; Siegel *et al.*, 1982). Thus, the ligand, siroheme, and iron−sulfur cluster should be viewed as a coupled electronic unit where an alteration in electronic or structural properties of one component will be reflected in the others. Direct or indirect influence of the protein on ligated states is reflected in an unusual property of the the low-spin CO complex, which cannot be photodissociated (Murphy *et al.*, 1974; Han *et al.*, 1989), even though the free siroheme−CO complex is readily photolyzed (Murphy *et al.*, 1974). Resonance Raman spectroscopy suggests that, when bound to the siroheme, the vibrational stretching frequencies of diatomic ligands are reduced by distal hydrogen bonds supplied by the protein and/or transfer of electron density from the Fe_4S_4 cluster (Han *et al.*, 1989). Charge transfer from the Fe_4S_4 cluster into carbon monoxide bound to the siroheme is further supported by a decrease in the C−O stretching frequency on reduction of the cluster (Han *et al.*, 1989).

The assimilatory SiRHP does not release any detectable intermediates when reducing either sulfite to sulfide or nitrite to ammonia (Siegel *et al.*, 1982; Janick *et al.*, 1983). Sulfite and nitrite both form low-spin ($S = {}^1/_2$) complexes with the ferric siroheme in SiRHP's active center that are largely EPR-silent (Day *et al.*, 1988) but give some "highly anisotropic low spin" (HALS) signals at $g = 2.5-3.0$ (Young & Siegel, 1988a). The 2.2 Å resolution structure of SiRHP in complex with sulfite revealed that sulfite binds the siroheme iron through sulfur and is coordinated by an array of protein-supplied positively charged side chains (Crane *et al.*, 1995). Siroheme-bound intermediates in the six-electron reductions of sulfite to sulfide or nitrite to ammonia by SiRHP are not well characterized, with the exception of a nitrosyl-ferroheme species trapped by stopped-flow freeze−quench EPR experiments after fully reduced SiRHP was reacted with nitrite (Janick *et al.*, 1983). During steady state turnover of nitrite by the sulfite reductase holoenzyme (consisting of SiRHP and an electron-suppling flavoprotein subunit), the nitrosyl-ferroheme complex is the dominant species observed; thus implicating nitric oxide as a reaction intermediate (Janick *et al.*, 1983). A change from triplet to doublet hyperfine splitting of the nitrosyl-ferroheme EPR resonance on substitution of $^{14}NO_2^-$ for $^{15}NO_2^-$ confirms that the nitrogen atom is bound to the siroheme iron derived from NO_2^-. A bent SFe−N−O bond is suggested by the rhombicity of the nitrosyl-siroheme EPR signals (Janick & Siegel, 1982) and confirmed by resonance Raman spectroscopy, which also indicates that distal hydrogen bonding from the protein to the ligated NO influences its vibrational modes (Han *et al.*, 1989). SiRHP can also reduce hydroxylamine (NH_2OH), which is a likely four-electron reduced intermediate in the six-electron reduction of nitrite to ammonia (Siegel *et al.*, 1982). A complex between SiRHP and hydroxylamine itself has never been observed spectroscopically.

Herein, we present crystallographic structures of SiRHP ligated with sulfite, nitrite, cyanide, carbon monoxide, nitric oxide, sulfide (or an oxidized derivative thereof), and an oxidized nitrogen species (probably nitrate). The ligand binding site, on the siroheme's distal face, has been constructed to provide preferred locations for recognizing the functional groups of ligands with varied size, shape and charge. Related stable coordination states for successively deoxygenated siroheme ligands are consistent with a reaction mechanism where substrate anions are sequentially reduced by two electrons and concurrently dehydrated while remaining bound to the siroheme.

EXPERIMENTAL PROCEDURES

Complex Preparation. SiRHP was purified as described previously (Siegel *et al.*, 1973; Kaufman *et al.*, 1993a; Crane *et al.*, 1997). Crystals were grown and complexes were prepared anaerobically in a Coy glove bag. SiRHP crystals were reduced by treatment with Cr(II) EDTA solutions or by irradiation in the presence of proflavin and EDTA (Crane *et al.*, 1997). The ability of these procedures to reduce SiRHP crystals was monitored with single-crystal EPR (Crane *et al.*, 1997).

(A) Preparation of HP−CO and HP−CN⁻. To complex SiRHP with CO or CN^-, crystals were treated with solutions containing 10 mM Cr(II) EDTA in the presence of dissolved carbon monoxide or 25 mM KCN. CO gas was bubbled through 3 mL solutions of 65 mM potassium phosphate buffer, pH 7.7, and 15% poly(ethylene glycol), molecular weight 8000 (KP_i/PEG), or 130 mM HEPES, pH 7.7, and 15% poly(ethylene glycol), molecular weight 8000 (HEPES/PEG), for 1−3 h. Cr(II) EDTA (10 mM) was then added to the solution before introduction of crystals, which were then soaked for periods of 30 min−36 h in sealed depression wells. These solutions converted soluble SiRHP to the SiRHP−CO complex in a few minutes (assayed optically). The SiRHP−CN^- complex was formed by incubating crystals in 100 μL of 25 mM KCN and 10 mM Cr(II) EDTA in KP_i/PEG for 30 min before the crystals were mounted dry in a glass capillary. These experiments were carried out in parallel with the reduction of SiRHP crystals in KP_i/PEG (HP−PO_4 CrII) and HEPES/PEG (HP_{Em} CrII), where reduction was followed by single-crystal EPR (Crane *et al.*, 1997). In the refined structures, carbon monoxide was found to replace phosphate at only half occupancy while cyanide replaced phosphate completely. To compensate for the partial CO occupancy, a diffraction data set that modeled a completely occupied CO complex was constructed from data

Table 1: Diffraction Data and Refinement Statistics for Various Oxidation and Ligation States of SiRHP[a]

structure	ligand[a]	oxid state[b]	res'n[c] (Å)	R_{sym}[d] (%)	$I/\sigma I$[e]	comp[f] (%)	R-factor[g] (%)	comp[h] (%)	rmsd geom[i]	waters[j]	$\langle B\rangle$[k] (Å^2)	$\langle\Delta r\rangle$[l] (Å)	PDB code
HP−CN[m]	CN^-	−2	2.00	6.6	14.0	97.5	18.8	94.7	0.010	374	23.2	0.19	4gep
			2.08−2.00	27.8	3.5	96.8	28.7	90.6	1.6				
HP−CO[m,n]	CO	−2	2.10	9.5	11.7	97.6	18.4	87.0	0.011	362	19.8	0.22	5gep
			2.18−2.10	28.6	3.7	96.4	24.6	55.4	1.6				
HP−SO_3[m]	HSO_3^-	0	1.90	7.0	17.9	97.5	17.5	93.5	0.009	350	25.3	0.17	2gep
			2.00−1.90	29.8	6.9	96.2	24.5	78.1	1.5				
HP−S[o,p]	$S(X)^{2-}$	0	2.40	9.6	14.0	92.1	17.3	91.1	0.010	297	26.8	0.30	7gep
			2.50−2.40	27.4	3.6	73.2	30.8	72.2	1.6				
HP−NO_2[m]	NO_2^-	0	2.10	7.8	16.4	98.9	18.5	96.2	0.010	352	31.1	0.23	3geo
			2.20−2.10	29.1	4.0	98.6	25.3	93.9	1.6				
HP−NO[m]	NO	−1	1.80	6.6	29.1	96.8	17.7	95.7	0.009	339	27.2	0.17	6gep
			1.90−1.80	23.0	4.2	95.6	25.0	93.3	1.5				
HP−NO_3[q]	NO_3^-	0 or −1	2.20	7.7	12.0	92.8	18.9	90.5	0.011	335	12.6	0.23	8gep
			2.40−2.20	33.8	2.1	83.5	23.9	79.7	1.6				

[a] Bound ligand. [b] Presumed predominant oxidation state relative to oxidized SiRHP (Fe^{3+} siroheme, $Fe_4S_4^{2+}$ cluster). [c] Maximum resolution of the diffraction data (upper entry), and range of resolution in the highest bin for compiling statistics (lower entry). [d] $R_{sym} = \sum\sum_j|I_j - \langle I\rangle|/\sum\sum_j|I_j|$, over all data (upper entry) and in highest resolution range (lower entry). [e] Intensity signal to noise ratio. [f] Completeness of unique diffraction data. [g] R-factor $= \sum||F_{obs}| - |F_{calc}||/\sum|F_{obs}|$. [h] Completeness of unique diffraction data used in refinement, with $|F| \geq 2\sigma|F|$. [i] Root mean square deviation of model bond lengths (upper entry, in angstroms) and angles (lower entry, in degrees) from ideal geometry. [j] Number of water molecules included in the refinement. [k] Average model thermal (B) factor. [l] Average coordinate error estimated from a σ_A-plot (Read, 1988). [m] Mar Research 30 cm image plate detector, SSRL beam line 7-1 (1.08 Å radiation), processed with DENZO (Otwinowski, 1993). [n] A fully occupied, reduced, carbon monoxide complex was refined against diffraction data extrapolated from diffraction data for a reduced crystal that contained both carbon dioxide and phosphate as axial ligands, each at partial occupancy, and a reduced crystal that only contained phosphate as an axial ligand [HP−PO_4 CrII; see Crane *et al.* (1997)]. [o] The HP−S complex is considered partially oxidized with an additional bonded atom (X) at a distance consistent with an oxygen. [p] Fuji image plates, SSRL beam line 1-5 (1.08 Å radiation), DENZO. [q] Siemens Hi-star multiwire area detector, Siemens SRA, XDS (Kabsch, 1988b).

collected on the partially occupied CO complex and data collected on the reduced phosphate complex [HP−PO_4 CrII (Crane *et al.*, 1997); see below].

(B) Preparation of HP−SO_3 and HP−NO_2. To form complexes of SiRHP with HSO_3^- and NO_2^-, crystals were soaked anaerobically for 3 days with either 50 mM Na_2SO_3 in HEPES/PEG, pH 7.9, or 100 mM $NaNO_2$ in HEPES/PEG, pH 7.7, respectively. Diffraction data for the SiRHP$^-SO_3^{2-}$ complex originally collected to a resolution of 2.2 Å with a Xentronics multiwire area detector mounted on a Rigaku Ru-200 rotating anode X-ray generator were superseded by a 1.9 Å resolution data set collected at the Stanford Synchrotron Radiation Laboratory (SSRL) (Table 1).

(C) Preparation of HP−NO. To produce the nitrosylferroheme complex, a SiRHP crystal was mounted in a capillary and photoreduced anaerobically with 750 μM proflavin and 50 mM EDTA in KP_i/PEG for a period of 40 min. After removal of the photoreducing solution, the crystal was dried with a paper wick and then bathed with 100 mM $NaNO_2$ in HEPES/PEG for 20 min in the dark. The crystal was then dried again and the capillary was sealed within the anaerobic glove bag.

(D) Preparation of HP−S. In an attempt to produce a complex with S^{2-}, a SiRHP crystal was incubated anaerobically in 40 mM Na_2S in HEPES/PEG for 48 h. Diffraction data were collected 36 h later at SSRL.

(E) Preparation of HP−NO_3. A putative complex of SiRHP with NO_3^- was produced when a crystal was bathed in a solution containing a high concentration of hydroxylamine. Analysis of diffraction data collected on a crystal soaked anaerobically for 36 h in 50 mM NH_3OHCl in HEPES/PEG suggested that a trigonal-planar molecule was bound in the SiRHP active center. The 50 mM NH_3OHCl in HEPES/PEG solution was analyzed for nitrate and nitrite content with Cayman's nitrate/nitrite assay kit (Alexis).

Approximation of Diffraction Data for a Fully Occupied SiRHP−CO Complex. Fourier maps (2.1 Å resolution) calculated with coefficients $F_o - F_c$ taken from the observed diffraction data collected on a putative SiRHP−CO complex and a SiRHP model not containing a distal ligand revealed a difference electron density peak consistent with phosphate and carbon monoxide each at partial occupancy.[2] Phosphate was added to the model and its occupancy was varied until difference maps produced a peak that only resembled carbon monoxide. This procedure suggested that the distal ligand binding site in the crystal was 0.5 ± 0.05 occupied by phosphate and 0.5 ± 0.05 occupied by carbon monoxide. To approximate a fully occupied diffraction data set for the SiRHP−CO complex (HP−CO_{ex}), the HP−CO data (Table 1) were first scaled to the diffraction data for HP−PO_4 Cr(II) with resolution-dependent single-parameter scaling in XtalView (McRee, 1992). The HP−PO_4 Cr(II) and HP−CO crystals were treated identically, except that CO was bubbled through the KP_i/PEG solution prior to soaking the HP−CO crystal. Following a procedure reported in Genick *et al.* (1997), we then evaluated the differences between each scaled and matched amplitude [$F_{HP-CO} - F_{HP-PO_4Cr(II)}$], doubled to compensate for the CO occupancy of 0.5, and added back to the HP−PO_4 Cr(II) amplitudes. The construction of this extrapolated data set assumes that the only contribution other than a SiRHP−CO complex to the HP−CO diffraction data is the reduced phosphate complex and that the HP−PO_4 Cr(II) diffraction data represent this species alone. The extrapolated amplitudes will only be an approximation for the true amplitudes of a fully occupied CO complex, because the phases associated with the HP−CO diffraction data are not considered. Essentially we correct

[2] Other attempts to form a completely occupied SiRHP−CO complex were unsuccessful. Crystals were incubated in CO-saturated KP_i/PEG and HEPES/PEG with 1−20 mM Cr(II) EDTA for 20 min to 48 h. Longer incubation times seemed to result in lower occupancies, suggesting that the rate of CO loss from solution was competing with the rate of CO diffusion into the crystal or the rate of siroheme reduction by Cr(II) EDTA. CO will bind to the reduced siroheme regardless of the cluster's oxidation state.

the F_{HP-CO} amplitudes by the scaled projection of the difference structure factor vector [$\mathbf{F}_{HP-CO} - \mathbf{F}_{HP-PO_4\ Cr(II)}$] onto $\mathbf{F}_{HP-CO}$. Because the differences in structure between the phosphate complex and the carbon monoxide complex are small compared to the conserved structural elements of SiRHP, and the phases of the difference vectors are random, the errors introduced by this approximation will be small. The SiRHP−CO complex was refined against this corrected diffraction data. There are advantages to refining the SiRHP−CO complex against the corrected diffraction data with contributions from the phosphate structure removed, as opposed to refining both phosphate and CO, each at partial occupancy, against the experimental data, which is a more standard approach. Effectively subtracting out the contribution from the HP−PO_4 Cr(II) structure from the diffraction amplitudes allows building of the CO into $F_o - F_c$ and $2F_o - F_c$ electron density that contains no contribution from the phosphate complex. Also, by correcting for every structure factor, our nonstandard approach is more similar to modeling two conformations for the entire protein model, not just for the ligands. Moreover, the correction is based on diffraction amplitudes for HP−PO_4 Cr(II) and is not dependent on a predetermined model.

Diffraction Data Collection and Reduction. Diffraction data for the various complexes and reduction states of SiRHP crystals were collected with a variety of synchrotron and conventional X-ray sources summarized in Table 1. The data sets, which ranged in resolution from 1.6 to 2.6 Å, were reduced with software that was appropriate and convenient for the data collection device and locality (Table 1).

Fourier Analysis, Model Building, and Refinement. Relative scaling of data sets and calculation of $2F_o - F_c$, $F_o - F_c$, and omit Fourier electron density maps were accomplished with the XtalView software package (McRee, 1992). XFIT, contained in XtalView, was used for model building and structural analysis. All refinement was carried out with X-PLOR (Brünger *et al.*, 1987). For the structure determinations of the SiRHP complexes presented below, a previously refined model of oxidized SiRHP at 1.6 Å resolution (Crane *et al.*, 1995; Crane & Getzoff, 1997), with the phosphate and water molecules removed, was refined by positional refinement in X-PLOR against the new diffraction data, first to 2.8 Å and then to 2.2 Å (or to the limit of the data's resolution). The loops and areas surrounding the active center were rebuilt to simulated annealed $F_o - F_c$ omit electron density maps (Hodel *et al.*, 1992), whereas the rest of the molecule, which changed little in conformation, was surveyed and adjusted with standard $F_o - F_c$ and $2F_o - F_c$ maps. Ligands were modeled into the resulting difference peaks on the distal side of the siroheme, resolution was extended, and water molecules were added gradually over cycles of positional conjugate gradient refinement, followed by *B*-factor refinement. Water molecules were placed only in difference peaks greater than 3σ that were 2.2−3.5 Å from appropriate protein hydrogen-bonding partners. The number of water molecules added was dependent on the resolution of the diffraction data (Table 1). In the last stages of refinement, where data quality and resolution permitted, restraints were completely removed from the iron−sulfur cluster, bridging ligand, and siroheme iron. When absence of high-resolution diffraction data limited the quality of refinement and made the configuration of the distal ligand somewhat ambiguous, multiple orientations and coordination geometries for the ligand were refined and evaluated for consistency with the difference density and suitable stereochemistry. In all complexes, the structural changes were small and localized to the active center and its surrounding loops.[3] Modeling of an overall anisotropic *B* value decreased the overall *R*-factor by up to 2% in some cases and improved the quality of difference maps, especially in regions surrounding the iron cofactors where large ripples were otherwise encountered in $F_o - F_c$ electron-density maps. Components of the overall anisotropic thermal factor were small but consistent for all of the reported structures and indicated slightly more disorder along b^* ($\langle B_{11}\rangle = -2.6$ Å^2, $\langle B_{22}\rangle = 3.3$ Å^2, $\langle B_{33}\rangle = -1.0$ Å^2). There is no obvious correlation between this anisotropy and the crystal shape or packing.

RESULTS

The various complexes of SiRHP presented in Table 1 are denoted in the text by HP (for hemoprotein) followed by abbreviations for ligand and oxidation state. Structural details for different reduction states of the enzyme in complex with phosphate (HP−PO_4) are reported in Crane *et al.* (1997).

Reduced SiRHP in Complex with CO and CN^-. Both carbon monoxide (Figure 1A) and cyanide (Figure 1B) bind to the siroheme iron at angles that are nearly perpendicular to the conjugated plane of the porphyrin. CO is inclined 9° toward Arg83 from the normal of the least-squares plane formed by the pyrrole and pyrroline nitrogens and has a SFe−C−O angle of 170°, whereas CN^- is inclined 8° toward Lys215 from the siroheme normal and has a SFe−C−N angle of 177° (Table 2). The nearly perpendicular binding of CO to the pyrrole−pyrroline plane of the two-electron reduced enzyme agrees with the coordination state predicted by resonance Raman spectroscopy (Han *et al.*, 1989). In an $F_o - F_c$ omit map produced with the HP−CN data and cyanide excluded from the calculated structure factors, the electron density peak principally suggests a perpendicular cyanide molecule; however, a $2F_o - F_c$ map produced with a perpendicular cyanide included in the model for the calculated structure factors suggests that there may be more than one conformation present and that one or more minority species are either slightly off-axis or bent. Although CN^- will bind the enzyme in all three oxidation states, we assume HP−CN is predominantly HP −2 because (i) it was reduced with CrII in parallel with HP−PO_4 CrII, which EPR evidence suggests is fully reduced (Crane *et al.*, 1997), (ii) cyanide replaced phosphate completely within minutes, whereas in the oxidized crystals ligand exchange for phosphate requires many days, (iii) the Cr(II) EDTA reagent, used in large excess, has a redox potential (∼−1.0 V) far below that of either cofactor [siroheme (−340 mV) and Fe_4S_4 cluster (−405 mV)], suggesting that if one of the two covalently linked cofactors can be reduced by this reagent, the other should be as well. However, resonance Raman spectroscopy indicates that different oxidation of the complex between

[3] Although *R*-Free (Brunger, 1993) was evaluated for the initial positional refinements of HP−SO_3, HP−PO_4 Cr(II), and HP−CO, all of the diffraction data were included in the high-resolution refinements so that the maximum amount of diffraction information would contribute to defining the cofactor and ligand geometry. Because the apparent structural changes in all complexes were localized to the active center and were relatively small compared to the overall structural consistency of the SiRHP protein moiety, phase bias introduced by the ligand-free oxidized SiRHP model was not a grave concern. *R*-Free was not a sensitive enough criterion to differentiate alternative bonding geometries of phosphate or sulfite to the siroheme.

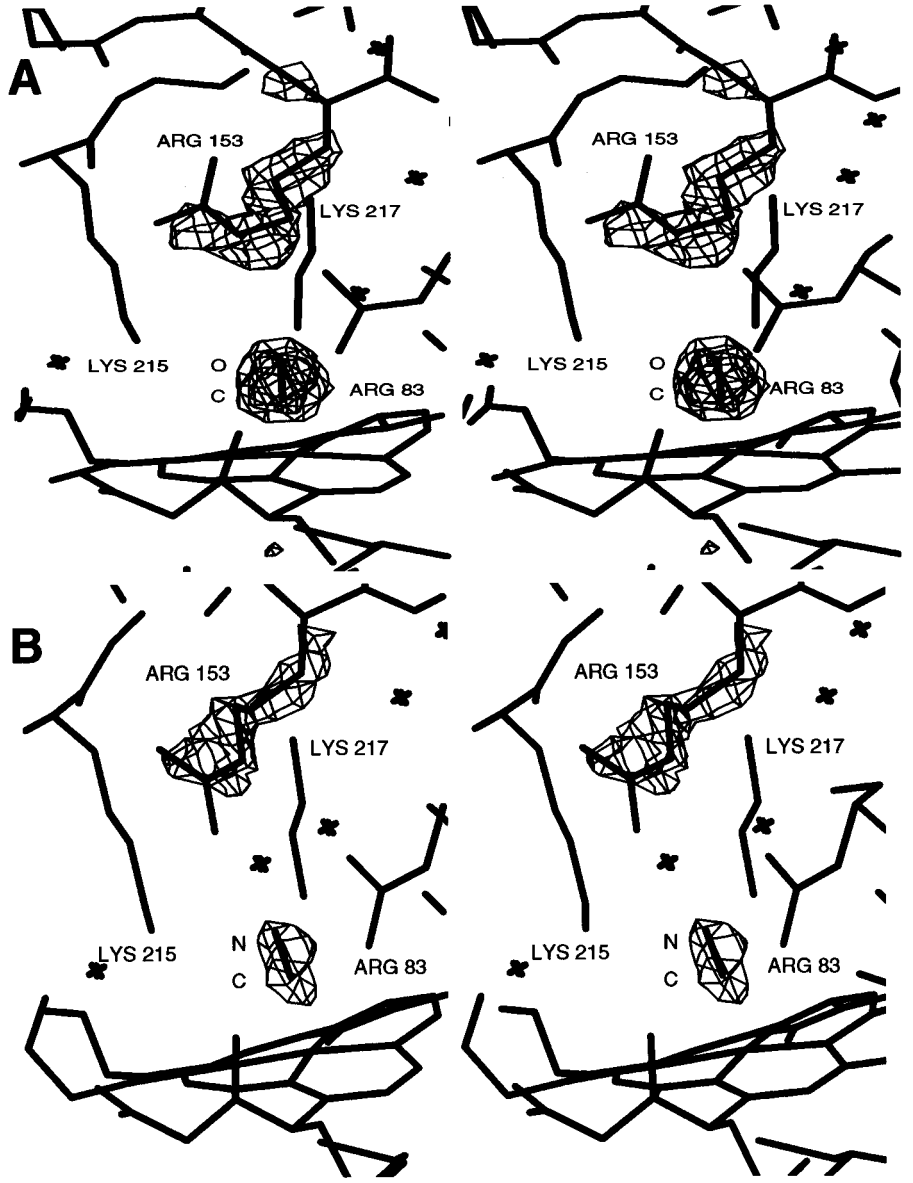
A
ARG 153
LYS 217
LYS 215
O
C
ARG 83
ARG 153
LYS 217
LYS 215
O
C
ARG 83
B
ARG 153
LYS 217
LYS 215
N
C
ARG 83
ARG 153
LYS 217
LYS 215
N
C
ARG 83

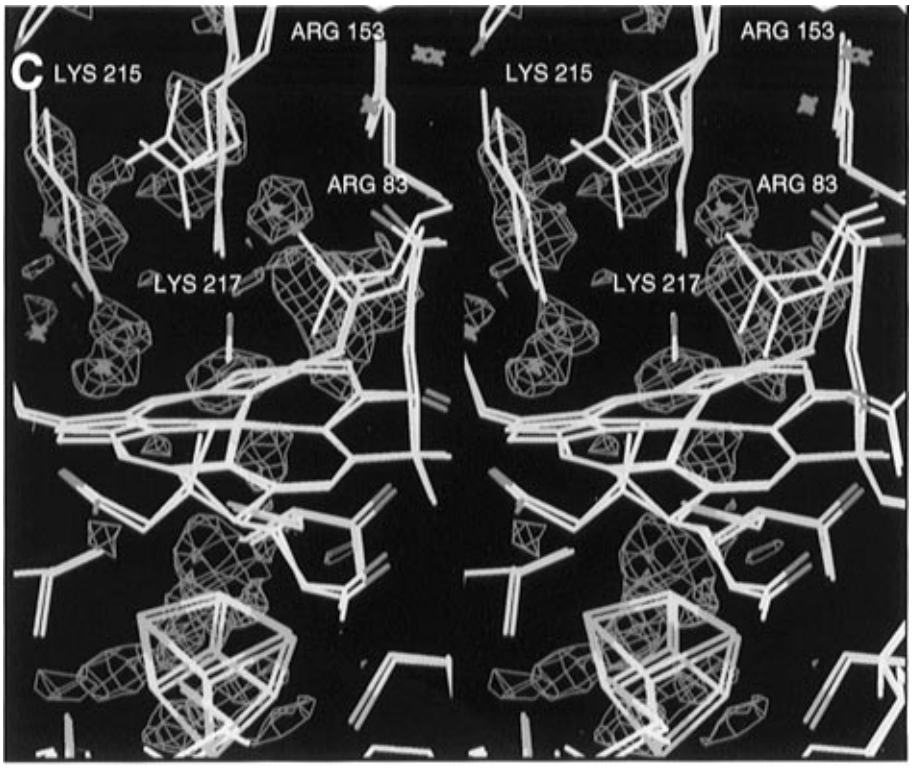
C
LYS 215
ARG 153
ARG 83
LYS 217
LYS 215
ARG 153
ARG 83
LYS 217

FIGURE 1: SiRHP in complex with inhibitors CO and CN^-. (A) Stereo view of electron density for carbon monoxide bound in the active site of SiRHP. Electron density contoured at 4σ and 6σ in a 2.1 Å resolution $F_o - F_c$ omit map, calculated without CO or Arg153 contributing to F_c, shows a small linear peak for carbon monoxide bound to the low-spin ferroheme (assumed through carbon) and a peak for Arg153 that places it too far away to hydrogen-bond to the CO oxygen (Table 3). The diffraction data for this complex was refined against data extrapolated from data for SiRHP reduced with Cr(II) EDTA and complexed with CO and HPO_4^{2-}, each at half occupancy, and from data for SiRHP reduced with Cr(II) EDTA and complexed with HPO_4^{2-} at full occupancy. See Experimental Procedures for details. The structure was subjected to 40 cycles of positional refinement in X-PLOR, without CO or Arg153, prior to the omit map calculations. (B) Stereoview of electron density for cyanide bound in the active site of SiRHP. Electron density contoured at 6σ in a 2.1 Å resolution $F_o - F_c$ omit map, calculated without CN^- or Arg153 contributing to F_c, shows an electron density peak consistent with a linear cyanide bound to the low-spin ferroheme (binding assumed through carbon) and density for Arg153 that indicates a closer interaction between the Arg153 guanidinium group and the bound ligand than in the HP−CO complex. The structure was subjected to 40 cycles of positional refinement in X-PLOR, without CN^- or Arg153, prior to the omit map calculations. (C) Difference electron density between the cyanide (cyan) and carbon monoxide (yellow) complexes. The 2.1 Å resolution electron density map was generated from the Fourier coefficients $F_{CN} - F_{CO}$ and phased with the refined cyanide-bound structure. Positive (blue) contours at 3.5σ indicate that the positively charged active-site side chains are generally closer to CN^- than to CO. Negative (red) contours at 3.5σ indicate that CO is bound closer to the siroheme iron than CN^-. Both the siroheme iron and the Fe_4S_4 cluster are displaced away from the distal binding site in the CN^- complex relative to the CO complex. All three panels were rendered with XFIT (McRee, 1992).

Table 2: Ligand and Cofactor Geometries for Various States of SiRHP

structure[a]	S−SFe[b] (Å)	S−Fe4[c] (Å)	SFe−L1[d] (Å)	SFe−Fe4[e] (Å)	CHB−S1[f] (Å)	SFe−S−Fe4[g] (deg)	SFe−L1−L2[h] (deg)	dome[i] SFE (Å)	⟨disp⟩[j] srm (Å)
HP−CN	2.23	2.31	1.84	4.12	3.84	130.5	171.0	0.09	0.28
HP−CO	2.23	2.29	1.62	4.06	3.87	127.9	167.0	0.13	0.32
HP−SO_3	2.34	2.28	2.20	4.17	3.66	128.9	113.3	0.11	0.37
HP−S	2.48	2.23	2.34	4.22	3.63	127.1	(131.6)	0.13	0.37
HP−NO_2	2.45	2.23	2.00	4.15	3.66	123.9	137.0	0.08	0.29
HP−NO	2.65	2.21	1.76	4.37	3.74	128.3	124.9	0.18	0.31
HP−NO_3	2.64	2.22	3.10	4.33	3.51	125.6		0.21	0.27

[a] See Table 1 for nomenclature and diffraction statistics of each crystal structure. [b] Bond length between the bridging cysteine thiolate of Cys483 (S) and the siroheme iron (SFe). [c] Bond length between the bridging cysteine thiolate of Cys483 (S) and the Fe_4S_4 cluster iron Fe4. [d] Bond length between the siroheme iron and the closest atom of the exogenous axial ligand (L1). [e] Separation between the siroheme iron and closest cluster iron (Fe4). [f] van der Waals contact distance between the siroheme meso carbon CHB and the cluster inorganic sulfur S1. [g] Angle defined by the siroheme iron, bridging sulfur, and covalently linked cluster iron. [h] Angle defined by the siroheme iron, the bound atom of the exogenous ligand (L1), and the ligand atom bonded to L1 (L2). For the sulfide complex [$S(X)^{2-}$], L2 is assigned to the sulfur's additional putative oxygen atom X and the value is given in parentheses. [i] Doming or displacement of the siroheme iron above the least-squares best plane formed by the pyrrole and pyrroline nitrogens of the siroheme. A positive displacement is in the direction of the distal-ligand binding position. [j] Average displacement of the 24 atoms in the isobacteriochlorin ring and the siroheme iron from their least-squares best plane.

SiRHP and CN^- have different coordination states (Han *et al.*, 1989), which raises the possibility of some contribution from a higher oxidation state in the HP−CN^- crystal.

Despite their structural similarity, CO and CN^- ligands have slightly different effects on the structure of the active center. As modeled, both CO and CN^- hydrogen bond to the buried water molecule at the back of the ligand-binding pocket that itself hydrogen-bonds to the siroheme's most axial propionate and Arg153 (Table 3). Since CO and CN^- are small and limited in their hydrogen-bond accepting ability, there is more disorder in the active-site side chains for the HP−CO and HP−CN structures than for structures containing larger ligands (Figure 2). Due to cyanide's negative charge, the positively charged active-site side chains are closer to CN^- than CO, and CN^- makes a hydrogen bond with Lys215, whereas CO does not (Figure 1C and Table 3). The interaction of CN^- with Lys215 may contribute to its different direction of inclination from the siroheme normal when compared to the coordination state of CO. Cyanide also binds further from the siroheme iron than carbon monoxide and appears to produce a downward movement of siroheme and Fe_4S_4 cluster away from the distal ligand-binding site (Figure 1C).

Substrate Complexes of Oxidized SiRHP. (A) Sulfite Complex. The 1.9 Å resolution structure of oxidized SiRHP in complex with the substrate sulfite (HP−SO_3) confirms and extends the conclusions drawn from the 2.2 Å structure presented previously (Crane *et al.*, 1995). In the HP−SO_3 structure, the siroheme iron (SFe) to Cys483 S^γ bond refines to 2.34 Å (Table 2), consistent with a low-spin configuration for the ferric siroheme iron. The S−O bond length for sulfite O3 is ∼0.2 Å longer that the other two S−O bonds and there is strong bridging electron density above 3σ from this oxygen to a water molecule (exp H_2O, Table 3) in the mouth of the active-site channel (Figure 3). Bound to the siroheme, sulfite participates in an extensive hydrogen-bond network with extended active-site side chains, the siroheme carboxylates, and ordered water molecules (Figure 4). The geometry about the sulfite sulfur is mainly tetrahedral, as is found with X-ray crystallographic structures of sulfite bound to transition metal ions (Ginn *et al.*, 1993).

The SiRHP−sulfite complex is more ordered crystallographically than the phosphate complex. The ordering of three loop regions (β4−α2, residues 127−131; α2−β5, 146−148; and eight residues of α3−β6, 184−185, and 204−209), all located in close proximity above the active center, is closely linked to side-chain rearrangements at the substrate binding site. The active-site ligating side chains contract down onto the sulfite anion, which, due to its coordination through sulfur, presents oxygen atoms that are ∼1.0 Å closer to the siroheme than those of the phosphate. The Arg153 guanidinium flips over to reach the sulfite but maintains a similar pattern of hydrogen bonding (Figure 5). This rearrangement of Arg153 breaks a hydrogen bond to the Met150 Sδ, allowing the loop containing residue 150 (α2−β5, 146−152) to coalesce and pack down against the new guanidinium conformation. This loop rearrangement shields the ligand-binding residues Arg83, Arg153, Lys215, and Lys217 from solvent but does not prevent solvent access to the siroheme-bound sulfite. A pocket connected to the

Table 3: Hydrogen-Bonding Distances and Separations between SiRHP Active-Site Residues and Bound Ligands

structure,[a] rsn (Å)	Arg83[b] N1, N2, Ne (Å)	Arg153[b] N1, N2, NE (Å)	Lys215[b] NZ (Å)	Lys217[b] NZ (Å)	srm[c] O2B (Å)	exp H_2O[d] (Å)	buried H_2O[e] (Å)
HP−CN	N 3.47		N 2.91	N 4.43			O 2.90
	N 4.09	N 3.35					
HP−CO	O 4.44		O 3.37	O 4.61			O 2.90
	O 4.23						
		O 3.71					
HP−SO_3	O2 3.02	O3 2.90	O1 3.01	O1 2.98		O3 2.60	O1 2.99
	O2 3.02		O3 2.85				O2 3.07
HP−S	S 3.80		X 3.08	X 3.28			X 2.30
	S 4.01	S 3.81	S 3.53	S 4.10			S 2.83
		X 3.72					
HP−NO_2	O2 3.70		O1 2.71	O1 3.06			O1 2.52
	O2 3.28	O2 3.66					O2 3.25
		O1 3.87					
HP−NO[f]		O_{c1} 2.82	O 3.13	O 3.72			O_{c1} 2.43
							O_{c2} 2.54
		O_{c2} 3.74					
HP−NO_3	O1 3.36		O1 2.93	O2 3.61	O2 3.02		
			O3 2.76	O3 2.82			
		O1 2.92					

[a] See Table 1 for nomenclature and diffraction statistics of each crystal structure. [b] Hydrogen-bonding distances and separations between bound ligands and the four active-site residues that contact them (Arg83, Arg153, Lys215, and Lys217). For Arg83 and Arg153 the hydrogen-bonding distances to the ligand atom specified in the table are given for Arg NH1 (N1), Arg NH2 (N2), and Arg NE in descending order. For lysine, all distances are between the specified ligand atom and Lys NZ. [c] Hydrogen-bonding distance to the siroheme's most axial propionate (oxygen O2B) on pyrroline ring B. [d] Hydrogen-bonding distance to an exposed water molecule (exp H_2O) that is positioned at the mouth of the active-site channel. [e] Hydrogen-bonding distance to a buried water molecule that interacts with the axial siroheme propionate oxygen (O2B) and fills the position of phosphate atom OP2 when the phosphate is absent. [f] In the NO complex, Arg153 and the buried H_2O were modeled in two conformations. Their interaction distances to the nitric oxide oxygen are specified to O_{c1} for conformation 1 and O_{c2} for conformation 2.

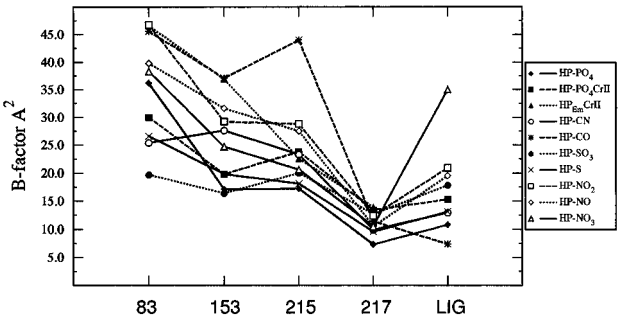

FIGURE 2: Refined thermal factors of active-site residue side chains and ligands in various states of ligated SiRHP. The average thermal factors (*B*-values) are shown for the four active-site side chains that contact ligands in the siroheme's distal axial coordination position (Arg83, Arg153, Lys215, and Lys217) and for the ligands themselves. For comparison, active-site thermal factors were normalized by the average overall thermal factor of the protein in each structure. Thermal factors are also reported for the oxidized enzyme with bound phosphate (HP−PO_4), the Cr(II)-reduced enzyme with bound phosphate (HP−PO_4 CrII), and the reduced enzyme with no distal ligand bound (HP_{Em} CrII) [see Crane et al. (1997) and Table 1 for the nomenclature, diffraction data, and refinement statistics associated with each species].

substrate binding cavity, containing seven ordered water molecules, is now sequestered from bulk solvent[4] (Figure 6). The stability inherent in this new packing arrangement is apparently propagated back along α2, ordering the loop between this helix and β4. As Arg83 is drawn toward the sulfite, both its side chain and the attached N-terminal β-strand become more rigid. To fill space to the distal side of the smaller sulfite anion, the Lys[215] aliphatic side chain swivels, and a water molecule appears above the sulfite, in the deep end of the substrate cavity (Figure 5). This water (buried H_2O, Table 3), buried from bulk solvent, hydrogen-bonds equally to two sulfite oxygens, as well as to Arg153 and the axial propionate from siroheme ring B (Figure 4). In the phosphate complex, this siroheme propionate hydrogen bonds to a protonated oxygen of the ligand itself.

(B) Nitrite Complex. In the complex between SiRHP and its alternate substrate nitrite, the electron density for the siroheme distal axial ligand is thin and fit well by an angular NO_2^- molecule bound to SFe through nitrogen (Figure 7) but is not consistent with NO_2^- bound to the SFe through oxygen. Nitrite, like sulfite, induces a movement of the siroheme iron into the plane of the porphyrin, which reflects a transition of the siroheme iron to low spin ($S = {}^1/_2$) (Young *et al.*, 1988a). In reaction with SiRHP, nitrite does not appear to first dehyrate to NO^+ before binding the siroheme iron, unlike reactions of nitrite with water-soluble porphyrin model systems (Barley *et al.*, 1986). Nitrite's O1 and O2 oxygen atoms occupy positions in the active site similar to sulfite's O1 and O2 oxygen atoms and make analogous hydrogen bonds to the protein (Table 3). Unlike sulfite, nitrite does not induce the rearrangement of Arg153 and the ordering of active-center loops on binding in the active site, and nitrite does not interact with a solvent-exposed water molecule in the mouth of the active-site channel. The "unflipped" orientation of the Arg153 guanidinium in the HP−NO_2 complex provides a closer association between nitrite's oxygens and both the NH1 and NE guanidinium nitrogens than would be allowed by the opposite, more extended "flipped" orientation observed in the HP−SO_3 complex.

A Reaction Intermediate: Nitrosyl SiRHP. X-ray diffraction studies of a photoreduced SiRHP crystal reacted with the substrate nitrite indicate the formation of a nitrosyl-ferroheme species in the active center of SiRHP. Analysis

[4] This cavity, on the side of Arg83 and Arg153 opposite to the siroheme, leads from bulk solvent to a water molecule that bridges the most axial siroheme carboxylate on pyrroline ring B to the peptide nitrogen of Asn154. Although conformational changes in Arg83 and Arg153 could provide access to the back of the distal anion binding pocket on ligand exchange, the ordered water molecule bridging Asn154 to the siroheme would have to be displaced, which seems unlikely considering its structural role in binding the siroheme to the protein (Figure 4).

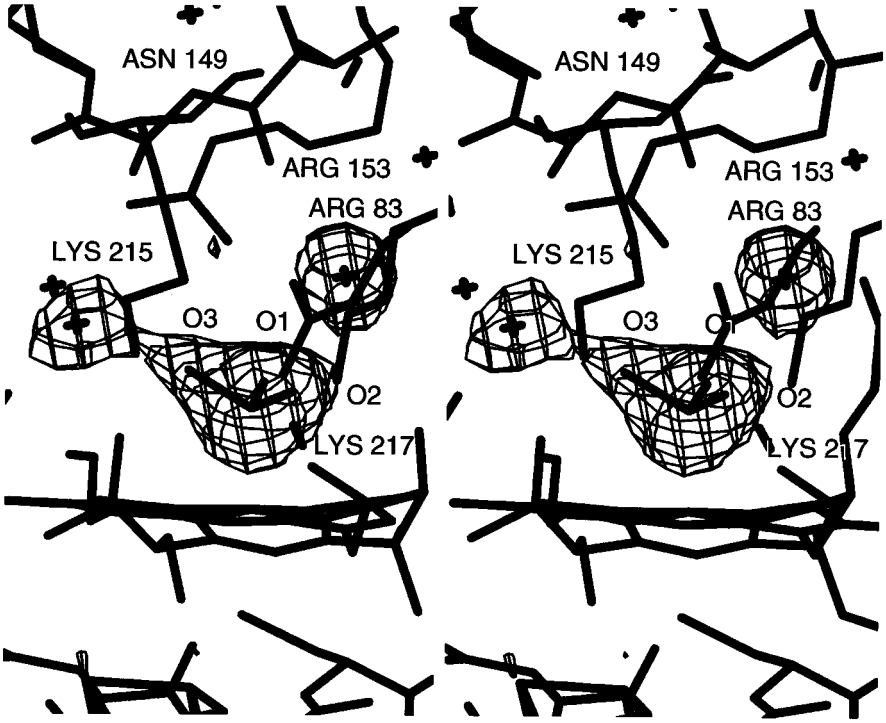

FIGURE 3: Stereoview of electron density for siroheme-bound sulfite and interacting water molecules. Sulfite binds through sulfur to the ferric siroheme iron of oxidized SiRHP and is also coordinated by Arg83, Arg153, Lys215, Lys217, and two water molecules (shown as crosses). Electron density contoured at 3.5σ in a 1.9 Å resolution $F_o - F_c$ omit map, calculated without sulfite or the interacting water molecules contributing to F_c, indicates both a buried water molecule (right) and a solvent-exposed water molecule (left). The O3 oxygen atom of sulfite forms a short (2.6 Å) hydrogen bond with this solvent-exposed water (see strong bridging density) and a long (1.7 Å) bond to the sulfite sulfur. Positional refinement of the model without sulfite was carried out for 40 cycles with X-PLOR before calculating the omit map. The figure was rendered with XFIT (McRee, 1992).

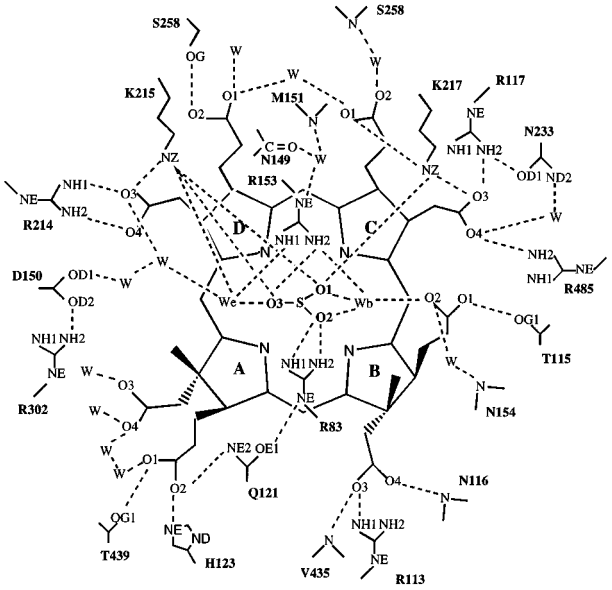

FIGURE 4: Active-site hydrogen-bond network of the complex between SiRHP and the substrate sulfite (HP−SO_3). Hydrogen bonds (dotted lines) of 2.6−3.2 Å length are shown between the substrate sulfite (atoms S, O1, O2, and O3), the siroheme (pyrrole rings A and B, pyrroline rings C and D), ordered water molecules (W), and active-site residues (one-letter amino acid abbreviations given with residue number and standard Protein Data Bank nomenclature for protein hydrogen-bonding atoms). An exposed (We) and a buried water molecule (Wb) interact directly with the sulfite's oxygen atoms. Viewpoint of the schematic diagram is roughly down the normal of the siroheme ring from the distal anion-binding site toward the proximal ligand Cys483 S$^\gamma$, with the siroheme iron residing below the bound sulfite sulfur and solvent access to the left of the diagram.

of the resulting 1.8 Å resolution diffraction data (Table 1) revealed omit electron density for a linear diatomic molecule bound to the siroheme iron with an inclined conformation (Figure 8), that is clearly different than for nitrite bound to the siroheme (Figure 7). This species, which in solution has been taken to represent an intermediate in the reduction of NO_2^- to ammonia (Janick *et al.*, 1983), has been modeled as a nitrosyl-ferroheme complex. The bound nitric oxide is bent, with the SFe−N−O angle refining to 125°, and the Cys483 S$^\gamma$−SFe bond has lengthened 0.2 Å compared to the HP−NO_2 structure (Table 2). The exposed loop between 146 and 148, which is ordered in the sulfite complex and disordered in the nitrite complex, remains disordered in HP−NO; and there is also more disorder in the positively charged active-site side chains compared to either of the substrate complexes. Particularly, Arg153 has been modeled in both the conformation found for HP−PO_4 and the flipped conformation found in HP−SO_3. In HP−NO, the NO is aligned between Lys215 and Lys217, along the N−O1 bond of the NO_2^- of HP−NO_2, and these residues hydrogen-bond to the NO oxygen with a geometry that mimics their interaction with O1 of NO_2^- in the nitrite complex (Table 3). The nitrosyl-siroheme species is likely ferrous because the NO−ferric heme complex is unstable (Janick *et al.*, 1983; Han *et al.*, 1989) and would not be expected to persist in the active site over the elapsed 48 h between the reaction of the crystal with substrate and data collection at SSRL. Although the formation of the nitrosyl-siroheme species suggests reaction of nitrite with HP −2, it is also possible that nitrite reacts with HP −1 to form a nitrosyl-ferriheme complex that is then reduced by a contaminating soluble reduction agent, such as the free copper, shown by EPR to be present in these samples (Crane *et al.*, 1997). Interestingly, compared to structures of other metal−nitrosyl complexes (Feltham & Enemark, 1981), the coordinaton

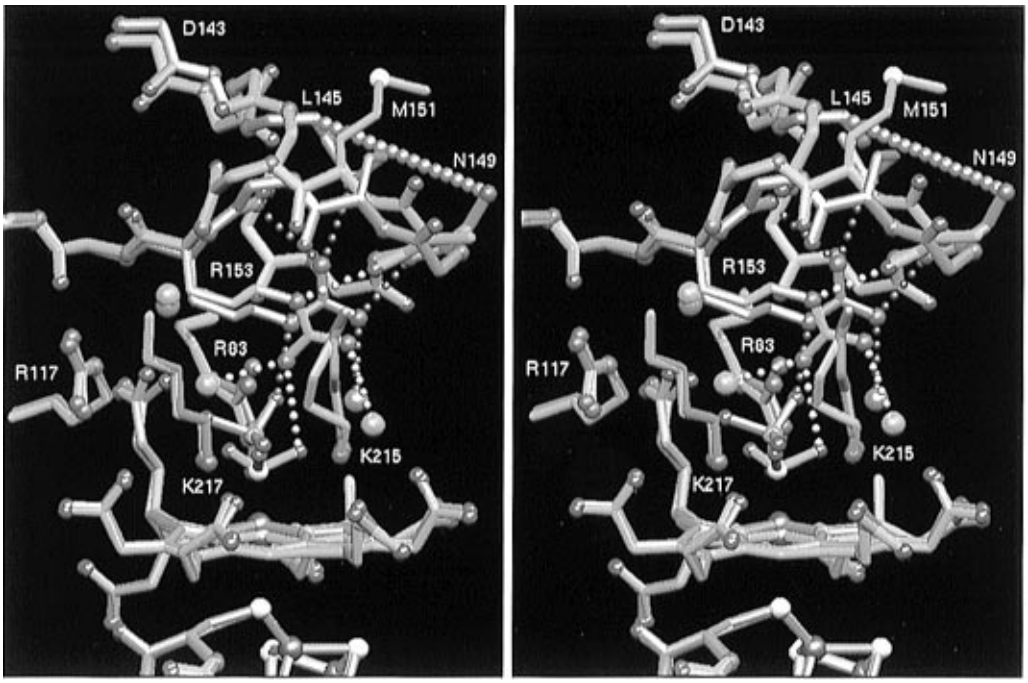

FIGURE 5: Stereo representation of the changes occurring in the SiRHP active center on the substitution of phosphate for the substrate sulfite. The phosphate complex (backbone, magenta; phosphorous, green; sulfur, yellow; nitrogens, blue; oxygens, red; iron, brown; hydrogen bonds, red) and sulfite complex (backbone, cyan; hydrogen bonds, yellow) were aligned by least-squares superposition of the Cαs from β5, β6, β3, β4, the subdomain 1 harness turn, and the domain 2 spiral connection. The guanidinium of Arg153 (center) flips over to bind the smaller sulfite anion yet maintains a similar arrangement of hydrogen-bonding partners. In the phosphate complex, residues 146−148 (represented by the dotted purple line) are disordered, while residues 149−151 exist in two conformations, one having the Met151 SD hydrogen-bonding to Arg153, an interaction that is broken when the Arg153 guanidinium flips on binding sulfite. The entire loop from 146 to 149 orders, packing down against the new arginine position. The ferric iron shifts into the plane of the pyrrole/pyrroline nitrogens on binding sulfite, reflecting its transition from high to lowspin. Along with the iron movement, a slight shift of Cys483 and the cluster closer to the siroheme produces a ∼0.4 Å shorter bond to the bridging thiolate. The aliphatic portion of the Lys215 side chain rotates to fill space vacated by the larger phosphate, and an additional water molecule (cyan sphere), appearing above the sulfite, takes the place of a hydrogen-bonding interaction between the phosphate and the most axial siroheme propionate. In both complexes, a structural water bridges the axial propionate to the Asn154 peptide nitrogen on β5, and another water molecule hydrogen-bonds closely to the phosphate or sulfite oxygen oriented towards bulk solvent (right). The figure rendered in AVS (Upson *et al.*, 1989).

geometry observed in HP−NO is more consistent with an Fe(II)−NO^- rather than an Fe(II)−NO species.

A Partially Oxidized Product Complex (HP−S). Attempts to produce a product complex of SiRHP with sulfide resulted in a ligated state where the exogenous sulfur siroheme ligand appears to be partially oxidized. Diffraction data collected from a SiRHP crystal soaked anaerobically in 40 mM sulfide for 48 h, revealed a large spherical difference density centered approximately 2.3 Å from the siroheme iron that was interpreted to represent S^{2-} bound as an axial ligand (Figure 9A). However, when sulfide was included in the model, an $F_o - F_c$ electron density map showed residual electron density in the ligand-binding site ∼1.7 Å from the refined position of S^{2-} (Figure 9B), suggesting contribution from an additional, minority ligand in the HP−S structure. This residual difference peak is unlikely to represent partial occupancy for a bound water molecule because no water molecule is found at this position in the unligated structure [HP_{Em} (Crane *et al.*, 1997)]. Neither is the peak shape consistent with partial occupancy of unexchanged phosphate. Rather, due to the short distance between this residual density peak and the siroheme-bound sulfur, we interpret the surplus density as belonging to an oxygen atom of a diatomic S−O species resulting from partial oxidation of S^{2-}. Sulfide is a strong reducing agent and thus is susceptible to oxidation in aqueous solution, even under anaerobic conditions (Wairavamurthy & Zhou, 1995).[5] However, given that this structure is limited to 2.4 Å resolution, there is some ambiguity to the identity of the diatomic species; for instance, an S−S bond of a partially occupied persulfide species could also be possible. Hence, the atom responsible for the residual density will be specified as X. Interestingly, this putative diatomic sulfur−oxygen species is oriented in the active site analogously to nitric oxide in the HP−NO structure. Although a monooxygenated form of sulfur would be extremely reactive, the SiRHP active center appears to stabilize otherwise unstable oxidation states of sulfur (Janick *et al.*, 1983). In the HP−S structure, the siroheme iron doming is consistent with the low-spin state measured by EPR for SiRHP complexed with sulfide (Janick & Siegel, 1982), although the bond between the Cys483 S^{γ} is intermediate in length between the high-spin phosphate complex and the low-spin substrate complexes (Table 2).

Oxidized SiRHP in Complex with Nitrate. Attempts at forming a complex of SiRHP with hydroxylamine resulted in an oxidized nitrogen anion in the active site that is not coordinated to the siroheme iron. Analysis of diffraction data collected from SiRHP crystals that were soaked anaerobically for 36 h in a solution of 50 mM NH_3OHCl in HEPES/PEG reveal an $F_o - F_c$ difference electron density peak above the siroheme iron that is trigonal planar in shape. The peak is modeled best by a nitrate anion (Figure 10). Analysis of the NH_2OH HEPES/PEG solution in which the crystal

[5] Diffraction data collected on SiRHP crystals that were incubated with sulfide for many days show large difference electron-density peaks in the active center that are difficult to interpret and are likely representative of admixtures of higher oxidized forms of sulfur (perhaps including thiosulfate and trithionate).

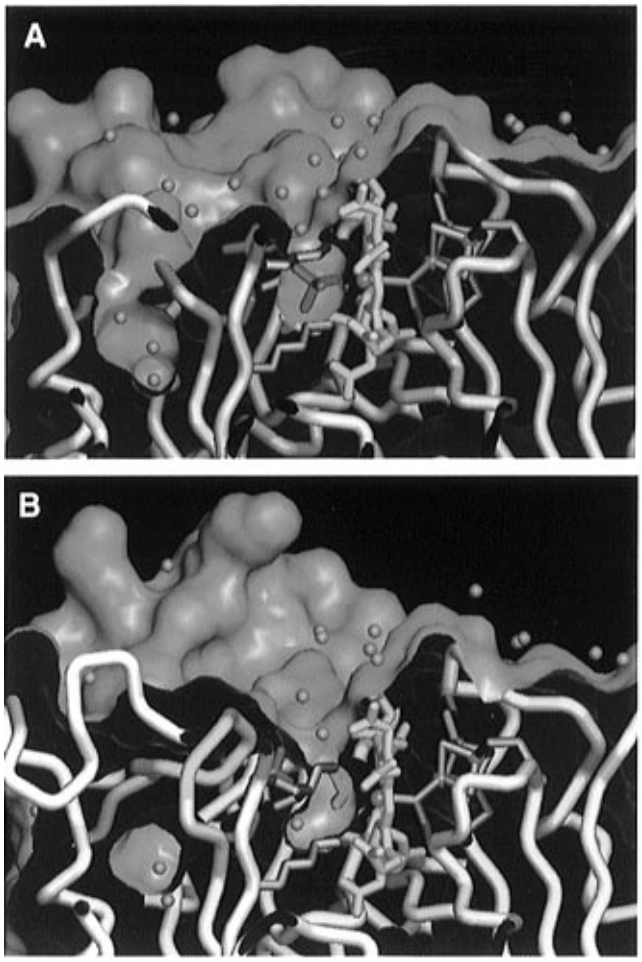

FIGURE 6: Comparison of the active-center cavity of oxidized SiRHP in complex with phosphate (A) and with sulfite (B). Compared to phosphate (purple, center), which coordinates the siroheme iron through oxygen, sulfite (bright green) coordinates to the siroheme (gold, center) through sulfur and in doing so causes the guanidinium of Arg153 (red) to flip and the siroheme iron (brown) to move into the plane of the porphyrin ring compared to the phosphate complex. A surface loop (yellow tube, left), disordered in the other complexes, orders and packs beside the active-site side chains that coordinate the sulfite. The shape of SiRHP's solvent-accessible surface (purple) around the active center is further changed by two other loops that also become ordered. These changes alter the positions of ordered solvent (blue spheres) filling the cavity and the shape of the anion binding pocket compared to the phosphate complex. Two ordered solvent molecules contact the sulfite oxygens, one at the back of the cavity (buried water molecule, bottom) and one at its mouth (exposed water molecule, center). The loop rearrangements that accompany sulfite binding also sequester a pocket connected to a substrate binding cavity that contains seven ordered water molecules (lower left).

was soaked found ~40−60 μM nitrate and 20−40 μM nitrite; however, crystals soaked for 1 week in a HEPES/PEG solution of 50 mM $NaNO_3$ failed to show any substitution of phosphate by nitrate or nitrite in the active center. A complex between the SiRHP and hydroxylamine has never been observed spectroscopically, although dismutation reactions of hydroxylamine with SiRHP have been observed.[6] Reduction of the SiRHP siroheme results in release of phosphate from the active site (Crane *et al.*, 1997). Thus, we speculate that reduction of the iron by hydroxylamine may facilitate the release of phosphate followed by binding of nitrate formed from spontaneous oxidation of hydroxylamine or as a byproduct of the dismutation reaction itself. The bound ligand in HP−NO_3 is coordinated by the active-site side chains in a manner analogous to the coordination of phosphate, with the exception that it does not bond to the siroheme iron (Table 3, Figure 10). The distance from the siroheme iron to Cys483 S^{γ} has decreased by ~0.2 Å relative to the phosphate complex (Table 2) but not by the ~0.5 Å seen in the structure of reduced SiRHP with an empty active site [HP_{Em} CrII (Crane *et al.*, 1997)]. In HP−NO_3, the domed configuration of the siroheme iron suggests a high-spin electronic state. Although the siroheme may be partially reduced in the HP−NO_3 complex, it is unlikely that the Fe_4S_4 cluster is reduced as well because there is excess hydroxylamine available to be turned over as substrate. The HP−NO_3 structure then contrasts with the HP_{Em} structure, which also lacks a sixth axial ligand but has an undomed siroheme iron and both cofactors reduced. Thus, it appears the displacement of the siroheme iron is influenced not only by the presence of an axial ligand but also by the oxidation state of the siroheme iron and possibly the oxidation state of the Fe_4S_4 cluster.

[6] L. J. Young and L. M. Siegel, unpublished data.

DISCUSSION

Uniquely Coupled Electron-Rich Cofactors and Their Interactions with Inorganic Ligands. Active-center structures of SiRHP in complex with small ligands of varying chemical character probe the electronic interactions among the coupled cofactors and bound ligands. A large *trans* influence of the exogenous ligand on the bond between the siroheme iron and the bridging thiolate (Table 2) emphasizes key features of the electronic coupling between cofactors for promoting catalysis. Although the spin state of the siroheme iron, the conformation of the siroheme macrocycle, and the oxidation states of both the siroheme iron and the iron−sulfur cluster could all potentially influence the bond distance between the siroheme iron and bridging Cys483 S^{γ}, structures of metalloporphyrin complexes indicate that, other than the chemical character of the ligand itself, the dominant factor determining the bonding distance of a given axial ligand is the character of the *trans* axial ligand (Scheidt & Gouterman, 1983). In SiRHP complexes where the siroheme iron is low-spin and roughly in the plane of the pyrrole and pyrroline nitrogens, shorter bond lengths between the proximal cysteine S^{γ} and the siroheme iron are unusually correlated with increasing π-acceptor character of the exogenous distal ligand. This bond length varies with distal ligand as CO, $CN^- < SO_3^{2-} < NO_2^- < S^{2-} <$ NO (Table 2). Usually, when π interactions between an iron porphyrin and a ligand are important for bonding, a better π-acceptor will back-bond with the metal and dominate its dπ orbitals, causing a weakening and lengthening of the bond between the metal and a second π-accepting axial ligand (Scheidt & Gouterman, 1983; Cotton & Wilkinson, 1988). With the exception of the NO complex (which has unique properties discussed below), this trend is reversed in SiRHP, where better π-acceptor ligands make the siroheme iron more positive and thereby decrease the length of the bond between it and the π-donating Cys483 S^{γ}. In addition, CO, being a better π-acceptor than isoelectronic CN^-, forms a shorter bond with the siroheme iron than CN^- and appears to draw the bridging

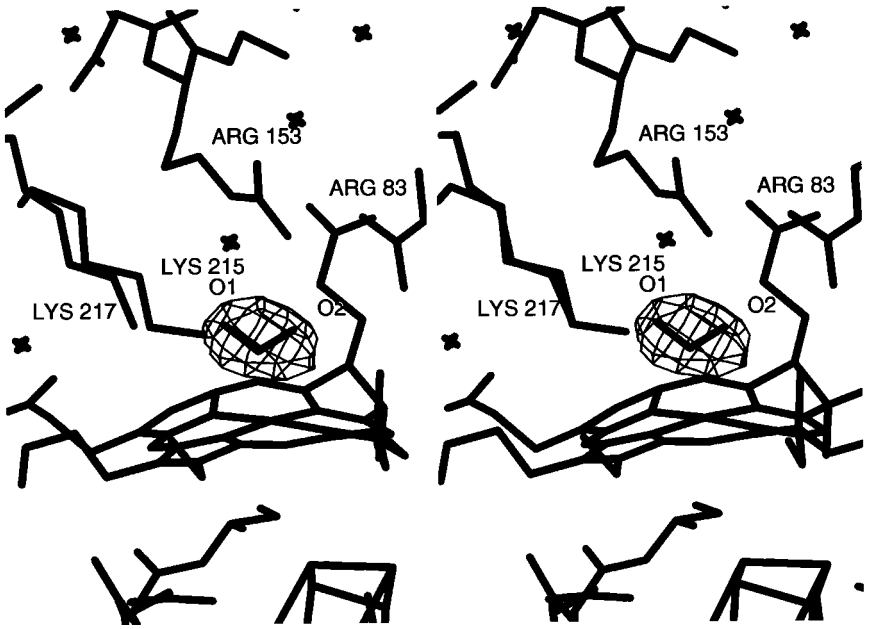

FIGURE 7: SiRHP in complex with nitrite. Stereoview of electron density for nitrite bound in the active site of oxidized SiRHP. Electron density contoured at 6σ in a 2.1 Å resolution $F_o - F_c$ omit map, calculated without any exogenous ligands contributing to F_c, shows a thin peak close to the siroheme with a size and shape consistent with an angular NO_2^- molecule. Lys215 and Lys217 are the closest coordinating protein ligands (see Table 3). Both nitrite oxygens hydrogen-bond to the active-site buried water molecule (cross above nitrite) at the back of the pocket, analogously to sulfite's interaction with a water molecule at this position. The HP−NO_2 structure was refined with X-PLOR for 40 cycles of positional refinement, without including NO_2^-, prior to calculation of the omit maps. The figure was rendered with XFIT (McRee, 1992).

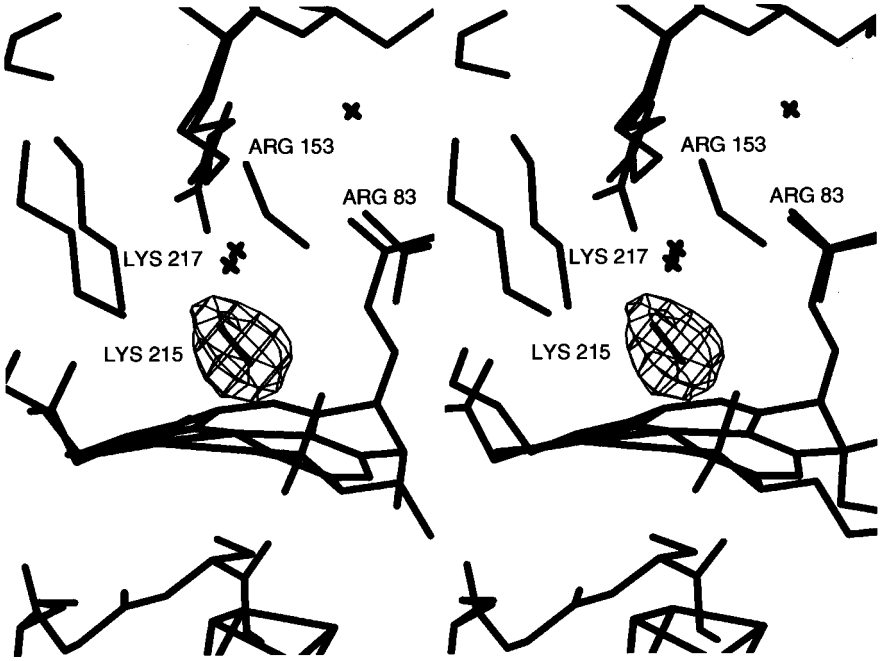

FIGURE 8: SiRHP with a bound reaction intermediate. Stereoview of a nitrosyl-ferroheme complex of SiRHP formed by reacting photoreduced SiRHP crystals with the substrate nitrite. The 1.8 Å resolution $F_o - F_c$ omit map contoured at 6σ, calculated without any exogenous ligands contributing to F_c, shows an oblong peak that is consistent with a linear NO molecule bound at an angle to the plane of the porphyrin. The peak is clearly different from the omit density for nitrite shown in Figure 7. Arg153 and the buried water molecule (cross above ligand) at the back of the active site were modeled in two conformations. One of the water positions is too close to the aliphatic side chain of Arg153 for the Arg's conformation to be only that of the phosphate complex. The HP−NO structure was refined with X-PLOR for 40 cycles of positional refinement, without including NO, prior to calculation of the omit maps. The figure was rendered with XFIT (McRee, 1992).

thiolate and Fe_4S_4 cluster toward the siroheme (Figure 1C).[7] Greater back-bonding between the siroheme dπ-orbitals and the ligand π*-orbitals in the CO complex compared to the CN^- complex is also supported by the ligand stretching frequencies observed by resonance Raman spectroscopy (Han *et al.*, 1989). Thus, the acceptance of π-electron density into the distal ligand may strengthen the siroheme's interaction with the bridging thiolate and therefore also with the iron−sulfur cluster. Density functional calculations on $Fe_4S_4^{1+}$ clusters reduced by one electron indicate that the highest occupied molecular orbital is largely Fe−S π-antibonding and that the additional negative charge is localized to the inorganic sulfurs and thiolate ligands (Noodleman & Case, 1992). If the electronic systems of the ligand, siroheme, and Fe_4S_4 cluster are highly conjugated in SiRHP, inductive electron flow into the π-antibonding orbitals of the ligand

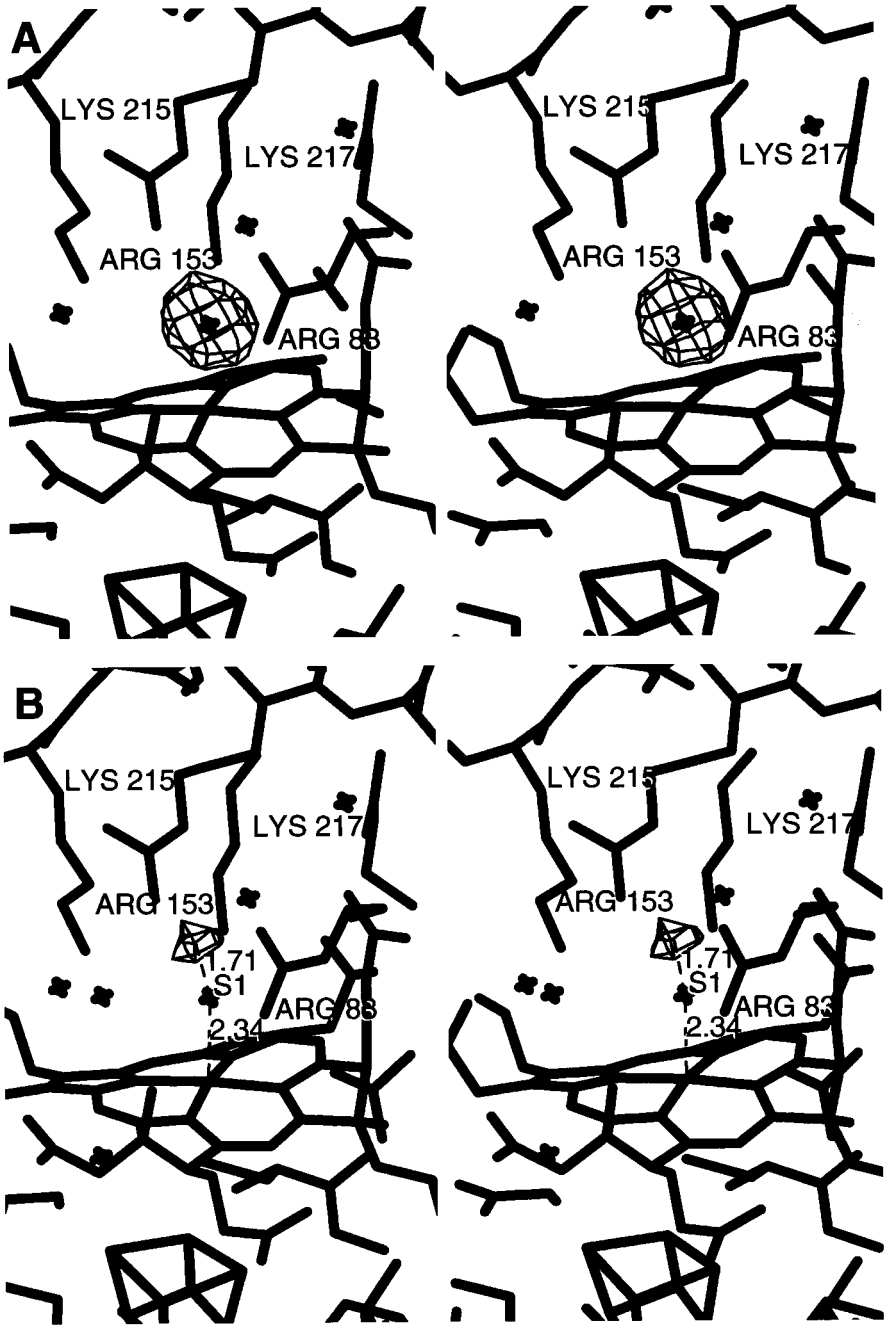

FIGURE 9: SiRHP with bound product. (A) Stereoview of electron density for a sulfide-like species bound in the active site of oxidized SiRHP. Electron density contoured at 6σ in a 2.4 Å resolution $F_o - F_c$ omit map, calculated without any exogenous ligand contributing to F_c, shows a large peak with a size and shape generally consistent with a sulfide anion bound 2.3 Å from the ferric siroheme iron that has moved into the plane of the porphyrin ring. However, the peak is slightly asymmetric. (B) Stereoview of a 2.4 Å resolution $F_o - F_c$ omit map contoured at 4σ and calculated from a model containing an S^{2-} (cross labeled S1) built into the difference peak of panel A. The remaining difference peak is 1.7 Å away from the sulfide and is at a position and angle similar to the oxygen of NO in the SiRHP−NO complex. Both panels were rendered with XFIT (McRee, 1992).

may manifest a shorter bond between the siroheme iron and the bridging thiolate by alleviating antibonding electron density between SFe and Cys483 S^{γ}. Transfer of electron density from the coupled cofactors into the substrate through π-back-bonding would increase charge on the substrate oxygens and populate antibonding ligand orbitals, thereby facilitating protonation and reductive cleavage of substrate-derived oxygen.

Conformational Change and Control of Substrate Binding, Activation, and Reactivity. Coordination of the substrate sulfite to the siroheme perturbs the protein moiety in a manner that likely facilitates the first stages of substrate reduction. Among the complexes examined, sulfite coordination to the siroheme causes the largest conformational change in the active center by inducing the guanidinium group of Arg153 to flip and the otherwise disordered loop between residues 146 and 152 to pack down against the

[7] This movement is not reflected in the unrestrained refined geometrical parameters of Table 2 which show equal distances between the bridging thiolate and siroheme iron for HP−CO and HP−CN; however, a small difference is beyond the sensitivity of the refinement, given the resolution of the diffraction data sets. It is also possible that traces of the HP−PO_4 Cr(II) structure remain in the HP−CO simulated data (see Experimental Procedures) that slightly skew the iron position in HP−CO toward a domed conformation.

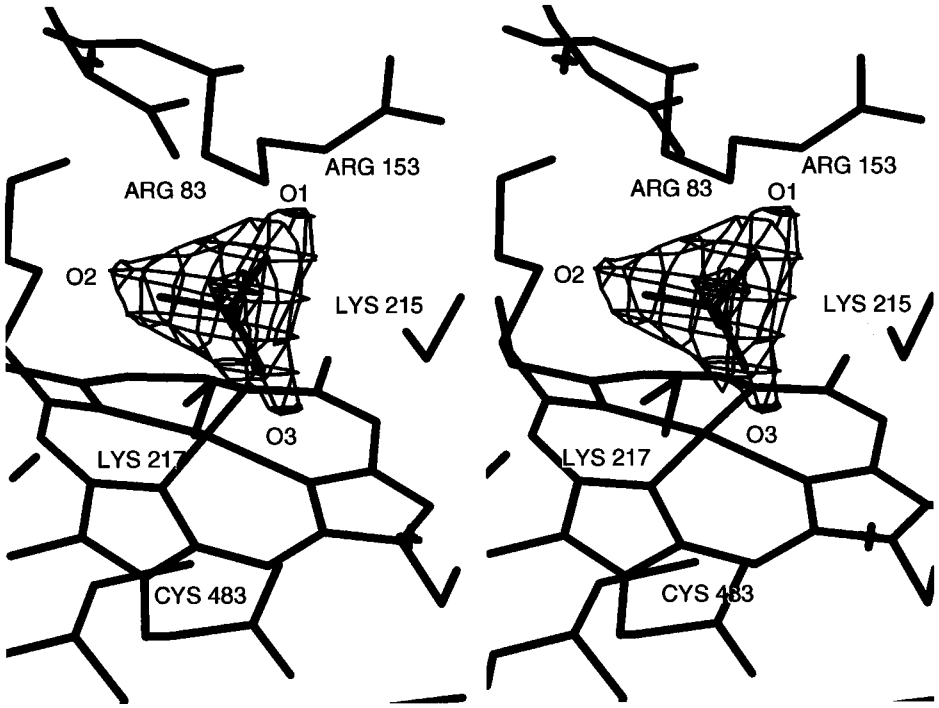

FIGURE 10: Stereoview of electron density for nitrate bound in the active site of oxidized SiRHP. Electron density contoured at 3.5σ and 8σ in a 2.2 Å resolution $F_o - F_c$ omit map, calculated without nitrate contributing to F_c, indicates that the trigonal planar NO_3^- molecule sits high above the siroheme in the binding pocket and does not bind to the siroheme iron. However, nitrate is strongly coordinated by Arg83, Arg153, Lys215, Lys217, an exposed water molecule (cross in foreground), and the axial pyrroline ring B propionate (upper left). Positional refinement of the model without Lys215, Lys217, or nitrate was carried out for 40 cycles with X-PLOR before calculaton of the omit map. The figure was rendered with XFIT (McRee, 1992).

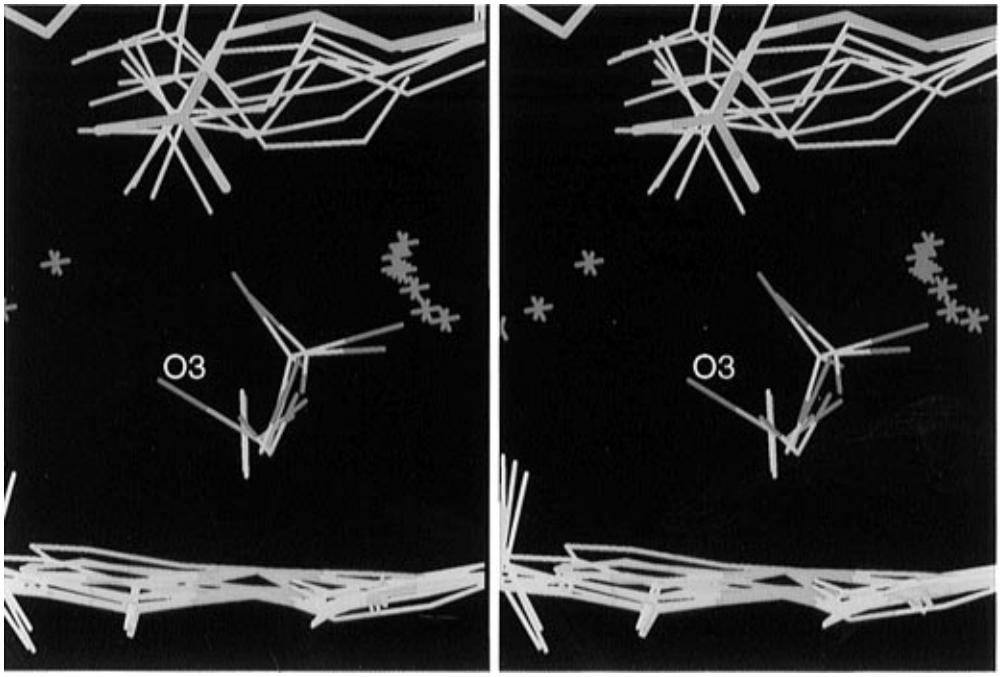

FIGURE 11: Unique coordination geometry of sulfite compared to other siroheme ligands. Stereo close-up of the overlaid siroheme-bound ligands phosphate, nitrate, sulfite, nitrite, nitric oxide, sulfide, carbon monoxide and cyanide (carbon, yellow and pink; oxygen, red; nitrogen, blue; sulfur, green; iron, brown) viewed down the edge of the siroheme (bottom) and orthogonal relative to the viewpoint of the figure. Only sulfite O3 interacts with the flipped conformation of Arg153 (thick pink lines, top right). The figure was rendered with XFIT (McRee, 1992).

guanidinium's new conformation (Figures 5 and 6). To trigger this conformational change, sulfite provides O3 in a unique position (compared to all the other ligated states) for hydrogen-bonding to the flipped guanidinium of Arg153 (Figure 11). The unique ordering of the active center in the HP−SO_3 complex may be why an activated form of the enzyme, produced by reduction in the absence of phosphate at high pH, will not release sulfite when it relaxes to an inactive state, but will release longer, more extended ligands, such as azide (Young & Siegel, 1988b). Polarization of sulfite's otherwise stable S−O bonds by the positively charged side chains of the active site is probably important for catalyzing reductive cleavage of the S−O bonds. The SiRHP active site supplies eight hydrogen-bonding interactions of 3 Å or less to the siroheme-bound sulfite (Table 3). Polarization of substrate S−O and N−O bonds may be

facilitated by a reduced dielectric constant within the active site, resulting from the shielding of Arg153 from solvent and sequestration of the active-site pocket by the coalescence of loop region 146−152 (Figure 6).

In contrast to the assimilatory sulfite reductases like SiRHP, which reduce sulfite to sulfide without releasing detectable intermediates, dissimilatory sulfite reductases primarily produce the incompletely reduced byproducts trithionate ($S_3O_6^{2-}$) and thiosulfate ($S_2O_3^{2-}$) (Peck & Lissolo, 1988). These products could result from attack of the nucelophilic sulfite molecule on partially reduced intermediates released from the active center or still bound to the siroheme. The loop movements observed in the SiRHP−sulfite complex constrain the positively charged active-site residues and limit accessibility of other substrate molecules to the active center during catalysis.

SiRHP and the assimilatory spinach nitrite reductase (SpiaNiR) are considerably homologous in their active-site residues and are each able to reduce both sulfite and nitrite (Crane & Getzoff, 1996); however, the two enzymes display catalytic properties that favor their preferred substrates. Moreover, unlike oxidized SiRHP, which binds heme ligands very slowly [$t_{1/2}$ ~8.5 h (Janick *et al.*, 1983)], the oxidized SpiaNiR exchanges heme ligands readily (Vega & Kamin, 1977). The alteration of Lys^{217} in SiRHP to Asn in SpiaNiR is the only sequence difference between the active-site residues that contact siroheme-bound ligands in these two enzymes. Lys217 is the most ordered ligand-binding side chain in all of the complexes examined (Figure 2). In HP−NO_2, as in HP−SO_3, Lys217 interacts closely with substrate oxygen O1 (3.0 Å, Table 3) and both carboxylates of the siroheme's pyrrole ring C (Figure 4). Barring any large rearrangement of the peptide backbone, Asn would be too small to maintain either the interaction with nitrite or the interaction with the siroheme. This suggests that in SpiaNir the structure of the distal anion binding site complexed with nitrite is different than in SiRHP or that the interactions provided by Lys217 are not important for productive binding of nitrite. Each enzyme binds its preferred substrate with a K_m of about 2 orders of magnitude less than that of the alternative substrate (Siegel *et al.*, 1982; Krueger & Siegel, 1982). Thus, removal of one charged hydrogen bond between Lys217 and sulfite appears to compensate for one less charged oxygen atom in nitrite. Discrimination against the smaller nitrite molecule by SiRHP may arise from a shortage of hydrogen bond acceptors to counter the many positive charges within the active center. As Lys217 is situated at the bottom of the substrate binding pocket, beneath the phosphate, the effect of Lys217 substitution on the ligand exchange rate is likely electrostatic rather than steric. Each enzyme is highly specific for its preferred substrate: the SpiaNiR k_{cat}/K_m is 3×10^5 greater for nitrite than for sulfite, while the SiRHP k_{cat}/K_m is 40× greater for sulfite than for nitrite (Siegel *et al.*, 1982, Krueger & Siegel, 1982). Even at substrate saturation nitrite is reduced ~10× faster by SpiaNiR than by SiRHP, while sulfite is reduced ~20× faster by SiRHP than by SpiaNiR. Thus, Lys217 may also be important for activating initial electron flow into sulfite or for stabilizing intermediates unique to the pathway of sulfite reduction. It is also interesting to note that, in the dissimilatory copper-containing nitrite reductase from *Achromobacter cycloclastes* that reduces nitrite to nitric oxide, the type II copper coordinates nitrite through its oxygen atoms (Adman *et al.*, 1995) and not through nitrogen, suggesting a considerably different catalytic mechanism than that of the siroheme-containing nitrite reductases.

Structure of a Nitrosyl-SiRHP Reaction Intermediate and Its Implications for Catalysis. The reaction of reduced SiRHP with nitrite results in formation of nitric oxide bound to the distal coordination site of the siroheme iron. The bonding configuration of nitric oxide is influenced by the conjugation of π-electron systems among the cluster, bridging cysteine thiolate, and the siroheme. Unlike CO and CN^-, which are isoelectronic and bond to the siroheme perpendicular to the porphyrin plane, nitric oxide has an additional electron that resides in a degenerate pair of pπ orbitals. In an angular bonding geometry with an iron porphyrin, these orbitals will mix with the iron's d_{z^2} orbital and result in a ligand-centered σ-bonding interaction (Palmer *et al.*, 1983).[8] Because this hybrid orbital is antibonding with respect to the other axial ligand, it may help to explain the increased separation between the Cys483 S^γ and the siroheme iron in the HP−NO complex compared to the HP−NO_2 complex (Table 2; S−SFe). In metalloporphyrin structures, the *trans* influence of an axial nitrosyl species also increases the bond between Fe(II) and the other axial ligands such as 1-methylimidazole and 4-methylpiperidine compared to the bisimidazole or bispiperidine complexes (Scheidt & Piciulo, 1976,Scheidt & Gouterman, 1983). The 125° angle of the SFe−N−O bond in the HP−NO structure suggests that there is considerable π-bonding between the bridging Cys^{483} S^γ and siroheme iron. The more linear the metal−N−O bond, the more the π-interactions between the iron and the nitrosyl ligand can be expected to contribute to bonding (Scheidt & Piciulo, 1976). The 10° decrease of the Fe−N−O angle in Fe(TPP)(NO)(1-MeIm) compared to Fe(TPP)(NO) has been suggested to result from decreased π-bonding between the iron and NO as a result of the *trans*-1-methylimidazole ligand (Scheidt & Frisse, 1975; Scheidt & Piciulo, 1976). Although there are no structures of nitrosyl-isobacteriochlorins on which to base comparisons, the 125° SFe−N−O angle in SiRHP is significantly smaller than the 149.2° Fe−N−O angle found in Fe(TPP)(NO) (Scheidt *et al.*, 1975), which suggests a strong *trans* influence of the bridging cysteine thiolate on the distal axial ligand in the HP−NO structure. However, the small SFe−N−O angle and long SFe−S^γ distance suggest an Fe(II)−NO^- rather than an Fe(II)−NO species in HP−NO (Feltham & Enemark, 1981). Further reduction of Fe(II)−NO in the crystal may have been possible by nitrite itself or reducing equivalents not removed after the photoreduction procedure.

The geometry of the SiRHP nitrosyl may also be influenced by the distal hydrogen bonds supplied by the protein and the electropositive character of the binding site. The considerably lower N−O stretching frequency in nitrosyl-SiRHP (1555 cm^{-1}) compared to nitrosyl-myoglobin (1624 cm^{-1}) is thought to reflect either increased hydrogen bonding to the distal NO oxygen in SiRHP or increased back-bonding to NO promoted by the electron-rich isobacteriochlorin ring or the covalently linked Fe_4S_4 cluster (Han *et al.*, 1989). The SiRHP active site provides extensive hydrogen-bond donors to NO, CO, and CN (Table 3), yet the decrease in C−O stretching frequency of SiRHP−CO on reduction of the Fe_4S_4 cluster [1920 cm^{-1} in HP −1 vs 1904 cm^{-1} in HP−2 (Han

[8] This bonding configuration can also be viewed as donation of an electron from the iron to NO and then sp^2 hybridization of the ligand to NO^-.

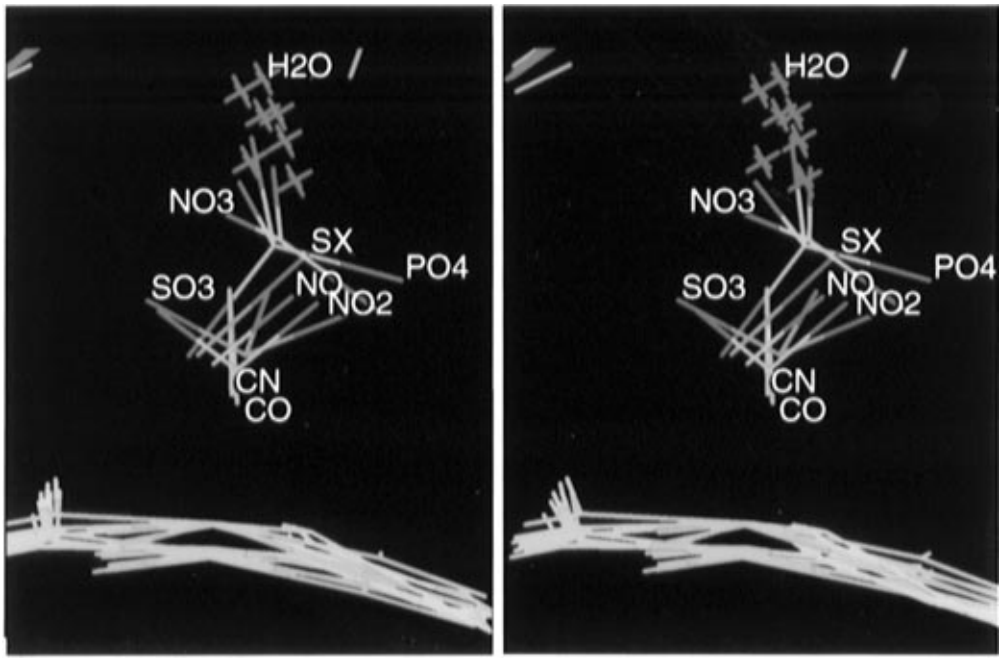

FIGURE 12: Preferred configurations of bound ligands in the active site of SiRHP. A stereoview of the siroheme bound ligands (orthogonal to Figure 11) emphasizes redundancy in their binding configurations (carbon, yellow and pink; oxygen, red; nitrogen, blue; sulfur, green; iron, brown). The oxygens of the planar nitrate anion substitute for three oxygens of the tetrahedral phosphate anion; the buried water (cross) takes the place of the oxygen atoms of phosphate and nitrate that hydrogen-bond to the axial siroheme propionate when smaller ligands are present; carbon monoxide and cyanide bind in almost identical fashion; the O1 and O2 of the angular nitrite molecule overlay with the O1 and O2 of the trigonal pyramidal sulfite molecule; the bent-binding configuration of the diatomic molecule nitric oxide mimics the N−O1 bond of nitrite and the S−O1 bond sulfite in the active site; and the putative monooxygenated sulfide-like species resembles nitric oxide in its binding geometry. The figure was rendered with XFIT (McRee, 1992).

et al., 1989)] demonstrates that the electronic state of the cluster also has an important influence over the internal bonds of bound diatomic ligands. It is likely the combination of distal hydrogen-bond donors and an assembly of electron-rich cofactors to promote the flow of charge into bound ligands that results in weakened internal bonds for species coordinated in the SiRHP active center.

A Proton-Rich Hydrogen-Bond Network That Recognizes Preferred Configurations of Bound Ligands. Comparisons of bound ligand configurations among the SiRHP complexes presented here reveal a striking conservation of ligand geometry and orientation in the distal-binding pocket (Figure 12). The redundancy in the coordinated orientations of tetrahedral ($HP-PO_4^{2-}$), trigonal pyramidal (HSO_3^-), trigonal planar (NO_3^-), angular (NO_2^-), and linear (NO, CO, SX, and CN^-) species demonstrates that the active site has been constructed to provide preferred locations for recognizing the functional groups of ligands with varied size, shape, and charge without requiring rearrangements of active-site residues or loops. This may be a requirement of an active center that must interact with species of varying shape, size, and charge generated during the multielectron reduction of substrate. Protein contributions to the hydrogen-bond network that coordinates bound anions in the active site is dominated by side-chain rather than main-chain interactions (Figure 4). Extended positively charged side chains provide a large number of torsional degrees of freedom for subtle rearrangement of bonding geometries that could allow the enzyme to stabilize catalytic intermediates at various stages of oxygenation. These positively charged protein residues provide a high effective proton concentration in the binding pocket to stabilize negative charge on the bound ligand and the siroheme carboxylate groups. The cage of lysine and arginine residues, the siroheme carboxylates, and structural water molecules form a hydrogen-bond network (Figure 4) with the flexibility to favorably interact with a variety of ligands bound to the distal coordination position of the siroheme. Structural water molecules potentially have two important roles in interacting with ligands: (1) to mediate, supplement, or substitute for interactions among the prosthetic groups, the protein and the exogenous ligands; thereby increasing the recognition potential of the binding site; and (2) to provide a direct or indirect source of protons for the generation of product water. The ruffled structure of the siroheme macrocycle, made possible by the saturated nature of the isobacteriochlorin ring, allows siroheme propionate groups to extend into the distal binding pocket and participate in hydrogen-bonding interactions with substrate (Figure 4). The most axial pyrroline propionate stabilizes the orientation of the buried water molecule that hydrogen-bonds to both sulfite and nitrite.

Structural States during Catalysis. The mechanism of sulfite reduction by SiRHP must involve delivery of electrons to substrate from the cofactors, protonation of substrate oxygen atoms, and release of product water molecules. The reduction and dehydration of substrate must be in part sequential because the prosthetic groups can be reduced by only two of the six electrons to be transferred to substrate at one time.[9] Thus, the active site of SiRHP must stabilize bound species that are successively deoxygenated over the course of reduction by six electrons. A mechanism for the reduction of sulfite by the low molecular weight assimilatory

[9] Although comparison of catalytic rates between the SiR holoenzyme with NADPH as an electron donor and the isolated hemoprotein with nonnatural electron donors suggests that electron transfer from NADPH to the coupled cofactors is rate-limiting in the holoenzyme (Siegel *et al.*, 1974; Siegel & Davis, 1974), different rates for for the reduction of HSO_3^-, NO_2^-, and NH_2OH by the SiR holoenzyme indicate that the rate of catalysis is not completely independent of substrate (Siegel *et al.*, 1974).

sulfite reductase has been suggested to involve sequential transfer of two electrons to the siroheme-bound sulfur and the concurrent cleavage of a leaving hydroxide group from substrate (Tan & Cowan, 1991;Lui *et al.*, 1993). In the SiRHP complexes examined, species likely to exist along the reduction pathway (SO_3^{2-}, NO_2^-, NO, and the putative partially oxidized SX ligand) mimic one another in their coordination geometry (Figure 12). Of these complexes, only the nitrosyl-ferroheme has been demonstrated to represent a true reaction intermediate (Janick *et al.*, 1983); however, the other species do represent stable coordination states for sulfur and nitrogen compounds with three, two, and one attached oxygen atoms. The strong bridging density between the protonated O3 of sulfite and a hydrogen-bonding water molecule only 2.6 Å away (Table 3, exp H_2O) may anticipate an early stage in the reaction where O3 is further protonated and reductively cleaved. Removal of this oxygen would likely leave a ferroheme$-SO_2^{\bullet -}$ or ferric heme$-SO_2^{2-}$ species in a geometry that resembles that of NO_2^- bound to the siroheme (Figure 12). Furthermore, a similar orientation for O1 of NO_2^- in the HP$-NO_2$ structure and the oxygen of NO in the HP$-$NO structure suggests that during the reduction of NO_2^- to NO by the enzyme, O2 of NO_2^- is reductively cleaved to water while the orientation of O1 is maintained. As NO is bound in the HP$-$NO structure with the same geometry as the putative partially oxidized SX species in the HP$-$S structure, identical coordination geometries may be manifested by both sulfite- and nitrite-derived intermediates over the course of catalysis.

A plausible reaction mechanism for the reduction of sulfite or nitrite by SiRHP would involve successive reduction and dehydration of substrates bound to the siroheme through either sulfur or nitrogen without release from the siroheme or substantial rearrangements of coordination geometry or the surrounding protein moiety. This is similar to the *push*$-$*pull* mechanistic paradigm used to describe O$-$O bond breakage during oxygen activation by heme-based oxygenases (Dawson, 1988; Poulos, 1988). In SiRHP, the electron-rich cofactors *push* electrons into substrate, while the high effective proton concentration provided by protein side chains and ordered solvent *pulls* charge onto the substrate oxygen atoms.

By analogy to the structures of SiRHP in the ligated and reduced states presented above and in Crane *et al.* (1997), we can envisage a series of structural states visited by the enzyme during the catalytic reduction of sulfite by six electrons (Figure 13). Assuming the resting state of SiRHP (Figure 13, **1**) to be the oxidized enzyme with HPO_4^{2-} bound to the siroheme, [see HP$-PO_4$, in Crane *et al.* (1997)], the first step in the reaction would involve reduction of the cofactors, followed by phosphate dissociation and an accompanying disordering of the positively charged, active-site side chains [Figure 13, **2**; see HP_{Em} in Crane *et al.* (1997)]. Sulfite would then bind to the siroheme as HSO_3^- (Figure 13, **3**), inducing the flip of Arg153 and the ordering of the active-site loops found in the structure of the oxidized SiRHP$-$sulfite complex (HP$-SO_3$). Electron transfer from the cofactors to substrate and proton transfer from the exposed active-site water molecule to the already singly protonated O3 of sulfite would result in the reductive cleavage of O3 from sulfite as water. Arg153 has reassumed its "unflipped" conformation for a closer interaction of the guanidinium NH1 and NE nitrogens with the remaining oxygen atoms of the deoxygenated sulfur intermediate

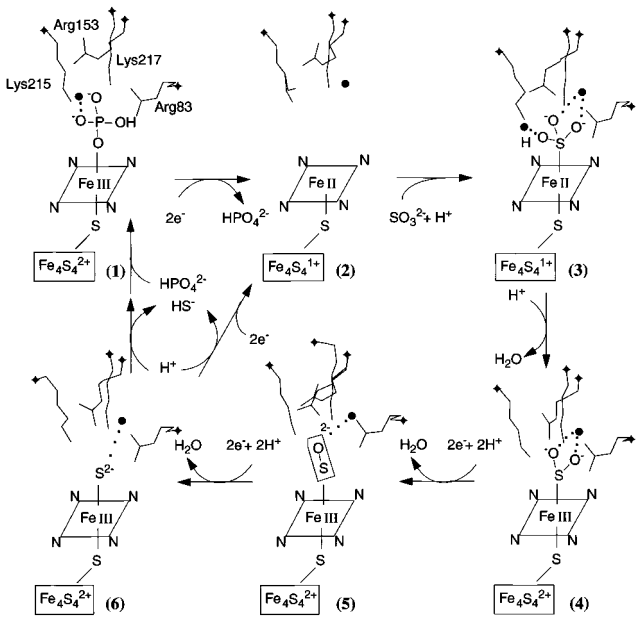

FIGURE 13: Schematic depiction of proposed SiRHP structural states during the catalytic six-electron reduction of sulfite. In the first step, **1** → **2**, reduction of the thiolate-coupled cofactors (siroheme represented by Fe boxed with pyrrole and pyrroline nitrogens and the iron$-$sulfur cluster represented by Fe_4S_4) results in release of phosphate from the active center and opening of the active site. In the next step, **2** → **3**, the binding of HSO_3^- is accompanied by the flipping of the Arg153 guanidinium and rearrangement of surface loops. Transfer **3** → **4**, of an additional proton from an ordered, exposed water (black dot, left) to singly protonated O3 of sulfite with concurrent electron transfer from the cofactors to substrate results in formation of water and dioxygenated sulfur. The Arg153 guanidinium assumes its "unflipped" conformation to better interact with the two remaining oxygens of the bound ligand. Two subsequent transfers, **4** → **5** and **5** → **6**, of two electrons and two protons to the coordinated species with loss of one water molecule at each step generates the product sulfide. Sulfide, being a poor siroheme ligand and less able to chelate multiple active-site residues, dissociates from the active center. During steady-state turnover it is probable that phosphate does not rebind to SiRHP following dissociation of HS^- from **6** prior to rereduction of the unligated oxidized SiRHP to **2**. Active-site water molecules (shown as black dots with hydrogen-bonding interactions to ligand oxygens as dotted lines) stabilize ligated states and probably provide protons for S$-$O bond cleavage and product water formation. In **4** → **5** and **5** → **6**, reduction of the cofactors is assumed to occur prior to proton transfer and release of water. Conformations for the active-site residues Arg83, Arg153, Lys215, and Lys217 are taken for **1** from the structure of HP$-PO_4$ (Crane *et al.*, 1997), for **2** from HP_{Em} CrII (Crane *et al.*, 1997), for **3** from HP$-SO_3$ (see Figure 3), for **4** from HP$-NO_2$ (see Figure 7), for **5** from HP$-$NO (see Figure 8), and for **6** from HP$-$S (see Figure 9A).

(Figure 13, **4**), in analogy to the complex of SiRHP with nitrite (HP$-NO_2$). Subsequent transfer of two electrons from the cofactors and two protons from the protein active-site side chains, or from the buried water molecule at the back of the active-site pocket, to the dioxygen species would release another water molecule and produce a monooxygenated sulfur species (Figure 13, **5**), in analogy to the SiRHP$-$nitric oxide complex (HP$-$NO) or SiRHP in complex with the putative monooxygenated sulfur species (HP$-$S). Additional transfers of two electrons and two protons and the release of water would generate the product sulfide, which is likely released from the active center as HS^- (Figure 13, **6**; see HP$-$S). Consistent with sulfide's electron-rich π-donating properties, it interacts more weakly with the SiRHP siroheme than most other π-accepting heme ligands (Janick & Siegel, 1982). Sulfide release from the enyzme

may also be facilitated by its smaller size and reduced charge, which diminish its chelation by multiple positively charged residues relative to sulfite and partially reduced substrate (Table 3).

The redundancy of preferred ligand configurations in the SiRHP active center suggests that the reduction of nitrite to ammonia by SiRHP involves similar structural states to those manifested during sulfite reduction. Nitrite binds to the ferric siroheme, through nitrogen, as NO_2^- rather than first dehydrating to NO^+. The flip of Arg153 and the loop ordering associated with sulfite binding do not occur with nitrite binding, suggesting that these perturbations are specifically necessary for the first step of sulfite reduction. Electron and proton tranfer to siroheme-bound nitrite results in dehydration and formation of Fe(II)−NO (analogous to step **4** → **5**, Figure 13). Although it has been noted that formation of Fe(III)−NO^- would be more consistent with a mechanism that involves three sequential two-electron reductions of nitrite (Lui *et al.*, 1993), EPR experiments indicate that Fe(II)−NO is the predominant species during the steady-state turnover of nitrite to ammonia by SiR (Janick *et al.*, 1983). Regardless of the exact electronic state of the NO complex, the next significant structural change in the active center will likely accompany the reductive cleavage of the remaining oxygen. Presumably the bound NO is first reduced to hydroxylamine (NH_3OH, four-electron reduced nitrite), which when provided as substrate can be reduced to ammonia by SiRHP. However, hydroxylamine has never been observed spectroscopically in complex with the enzyme.[10] If hydroxylamine is an intermediate on the reaction pathway, the final oxygen is likely released during the third two-electron reduction of NH_3OH to NH_4^+ (analogous to step **5** → **6**, Figure 13). Because conversion of Fe(II)−NO to Fe(III)−NH_3OH is a three-electron reduction, either single electron transfers from the cofactors are involved or an extra electron is derived from the siroheme ring by formation of a π-cation radical. The reaction sequence of Figure 13 does not consider the participation of higher-valent porphyrin cation species. Such π-cation radicals have yet to be observed during catalysis but are more favored by the reduced nature of the partially saturated isobacteriochlorin ring then they are by more oxidized heme groups (Chang& Fajer, 1980; Fujita & Fajer, 1983). Although the exact sequence and timing of electron and proton transfers from the enzyme to either sulfite or nitrite for the most part remain to be established, one would expect that electrons and protons are transferred in a concerted fashion to reduce the activation energy for bond cleavage.

The SiRHP active center is unique in the large number of positively charged residues contained in its substrate binding site. In addition to providing a positive electrostatic potential to polarize substrate bonds and stabilize the carboxylates of the siroheme, an important role for the active-site lysines and arginines may be to either directly provide protons for the formation of product water molecules or to activate ordered water molecules to do so. Proton transfer to iron-bound peroxide is thought to be a key feature in the O−O bond cleavage leading to oxygen activation by heme-containing oxygenases such as cytochrome P-450 (Sono *et al.*, 1996). Mutational studies of cytochrome P-450_{CAM} with nonnative amino acids suggest that active-site water molecules may be direct proton donors to iron bound peroxide for oxygen activation (Kimata *et al.*, 1995). The conformation of Arg153, particularly the orientation of its guanidinium group, is highly sensitive to the type of ligand bound and may be linked to proton flux or water exchange in the active center during catalysis. With the exception of loop rearrangements accompanying sulfite binding that sequester substrate and likely aid the first steps of reduction, the SiRHP active center changes little in conformation depending on the ligand bound. An active center that does not require large rearrangements over the course of catalysis may allow the reaction to proceed quickly and may also limit the accessibility of nucleophilic substrate molecules to reactive intermediately reduced species bound to the siroheme. The drastic switch in substrate preference between the assimilatory sulfite and nitrite reductases that appears to result from a single amino acid change (Lys to Asn) in the active center suggests that, in addition to the large positive potential and high proton concentration at the distal anion-binding site, specific hydrogen-bonding interactions are required for effective catalysis by SiRHP.

[10] Our attempts to form the hydroxylamine complex in SiRHP crystals resulted in the nitrate complex, HP−NO_3.

ACKNOWLEDGMENT

We thank S. L. Bernstein for her assistance with and efforts in improving the purification of over-expressed SiRHP; J. Wu and N. M. Kredich for providing the *E. coli* sulfite reductase expression system; J. A. Tainer, D. B. Goodin, T. G. Spiro, J. J. Rack, H. B. Gray, and N. M. Kredich for valuable discussions and advice; and the Stanford Synchrotron Radiation Laboratory for the use of data collection facilities.

REFERENCES

Adman, E. T., Godden, J. W., & Turely, S. (1995) *J. Biol. Chem. 270*, 27458−27474.
Barley, M. H., Takeuchi, K. J., & Meyer, T. J. (1986) *J. Am. Chem. Soc. 108*, 5876−5885.
Brünger, A. T. (1993) *Acta Crystallogr. D49*, 24−36.
Brünger, A. T., Kuriyan, J., & Karplus, M. (1987) *Science 235*, 458−460.
Chang, C. K., & Fajer, J. (1980) *J. Am. Chem. Soc. 102*, 848−851.
Cotton, F. A., & Wilkinson, F. (1988) *Advanced Inorganic Chemistry*, 5th ed., John Wiley, New York.
Crane, B. R., & Getzoff, E. D. (1996) *Curr. Opin. Struct. Biol. 6*, 744−756.
Crane, B. R., & Getzoff, E. D. (1997) *Acta Crystallogr. D53*, 23−40.
Crane, B. R., Siegel, L. M., & Getzoff, E. D. (1995) *Science 270*, 59−67.
Crane, B. R., Siegel, L. M., & Getzoff, E. D. (1997) *Biochemistry 36*, 12101−12119.
Dawson, J. H. (1988) *Science 240*, 1308−1319.
Day, E. P., Peterson, J., Bonvoisin, J. J., Young, L. J., Wilkerson, J. O., & Siegel, L. M. (1988) *Biochemistry 27*, 2126−2132.
Feltham, R. D., & Enemark, J. H. (1981) *Top. Stereochem. 12*, 155−215.
Fujita, E., & Fajer, J. (1983) *J. Am. Chem. Soc. 105*, 6743−6745.
Genick, U. K., Borgstahl, G. E. O., Ng, K., Ren, Z., Pradervand, C., Burke, P., Srajer, V., Tend, T., Schildkamp, W., McRee, D., Moffat, K., & Getzoff, E. D. (1997) *Science 275*, 1471−1475.
Ginn, V., Kelly, P. F., Papadimitiou, C., Slawin, A. M. Z., Williams, D. J., & Woollins, J. D. (1993) *J. Chem. Soc., Dalton Trans. 12*, 1805−1810.
Han, S., Madden, J. F., Siegel, L. M., & Spiro, T. G. (1989) *Biochemistry 28*, 5477−5485.
Hodel, A., Kim, S. H., & Brünger, A. T. (1992) *Acta Crystallogr. A48*, 851−858.
Janick, P., & Siegel, L. M. (1982) *Biochemistry 21*, 3538−3547.

Janick, P., & Siegel, L. M. (1983) *Biochemistry 22*, 504−515.
Janick, P. A., Rueger, D. C., Krueger, R. J., Barber, M. J., & Siegel, L. M. (1983) *Biochemistry 22*, 396−408.
Kabsch, W. J. (1988) *J. Appl. Crystallogr. 21*, 916−924.
Kaufman, J., Spicer, L. D., & Siegel, L. M. (1993) *Biochemistry 32*, 2853−2867.
Kimata, Y., Shimada, H., Hirose, T., & Ishimura, Y. (1995) *Biochem. Biophys. Res. Commun. 208*, 96−102.
Krueger, R. J., & Siegel, L. M. (1982) *Biochemistry 21*, 2892−2904.
Lui, S. M., Soriano, A., & Cowan, J. A. (1993) *J. Am. Chem. Soc. 115*, 10483−10486.
McRee, D. E. (1992) *J. Mol. Graphics 10*, 44−46.
Murphy, M. J., Siegel, L. M., & Kamin, H. (1974) *J. Biol. Chem. 249*, 1610−1614.
Noodleman, L., & Case, D. A. (1992) *Adv. Inorg. Chem. 38*, 423−469.
Otwinowski, Z. (1993) in *Data Collection and Processing* (Sawyer, L., Isaacs, N., & Bailey, S., Eds.) pp 56−62, Science and Engineering Research Council, Warrington, UK.
Palmer, G. (1983) in *Iron Porphyrins, II* (Lever, A. B. P., & Gray, H. B., Eds.) pp 217−286, Addison-Wesley, Reading, MA.
Peck, H. D., Jr., & Lissolo, T. (1988) in *Forty-Second Symposium of the Society for General Microbiology—The Nitrogen and Sulphur Cycles* (Cole, J. A., & Ferguson, S. J., Eds.) Vol. 42, pp 99−132, Cambridge University Press, Cambridge, England.
Poulos, T. L. (1988) in *Heme Proteins* (Eichorn, G. L., & Marzilli, L. G., Eds.) Vol. 7, Elsevier, New York.
Read, R. J. (1988) *Acta Crystallogr. A42*, 140−149.
Scheidt, W. M., & Gouterman, M. (1983) in *Iron Porphyrins, Part I* (Lever, A. B. P., & Gray, H. B., Eds.) Vol. 4, pp 89−140, Addison-Wesley, Reading, MA.
Scheidt, W. R., & Frisse, M. E. (1975) *J. Am. Chem. Soc. 97*, 17−21.
Scheidt, W. R., & Piciulo, P. L. (1976) *J. Am. Chem. Soc. 98*, 1913−1919.
Siegel, L. M., & Davis, P. S. (1974) *J. Biol. Chem. 249*, 1587−1598.
Siegel, L. M., Davis, P. S., & Kamin, H. (1974) *J. Biol. Chem. 249*, 1572−1586.
Siegel, L. M., Murphy, M. J., & Kamin, H. (1973) *J. Biol. Chem. 248*, 251−264.
Siegel, L. M., Rueger, D. C., Barber, M. J., Krueger, R. J., Orme-Johnson, N. R., & Orme-Johnson, W. H. (1982) *J. Biol. Chem. 257*, 6343−6350.
Sono, M., Roach, M. P., Coulter, E. D., & Dawson, J. D. (1996) *Chem. Rev. 96*, 2841−2887.
Tan, J., & Cowan, J. A. (1991) *Biochemistry 30*, 8910−8917.
Upson, C., Faulhabe, T., Kamins, D., Laidlaw, D., Schlegel, D., Vroom, J., Gurwitz, R., & Vandam, A. (1989) *IEEE Comp. G. 9*, 30−42.
Vega, J. M., & Kamin, H. (1977) *J. Biol. Chem. 252*, 896−909.
Wairavamurthy, M., & Zhou, W. (1995) *ACS Symp. Ser. 612*, 280−292.
Young, L. J., & Siegel, L. M. (1988a) *Biochemistry 27*, 2790−2800.
Young, L. J., & Siegel, L. M. (1988b) *Biochemistry 27*, 4991−4999.

BI971066I